The Linnean Society of London
ZOOLOGICAL Journal of the Linnean Society

Increasing the theropod record of Europe: A new basal spinosaurid from the Enciso Group of the Cameros Basin (La Rioja, Spain). Evolutionary implications and palaeobiodiversity.

Journal:	*Zoological Journal of the Linnean Society*
Manuscript ID	ZOJ-05-2023-5383.R1
Manuscript Type:	Original Article
Keywords:	Theropoda < Taxa, Dinosauria < Taxa, Early Cretaceous < Palaeontology, Europe < Geography, palaeobiogeography < Geography, biodiversity < Ecology, Evolution
Abstract:	A new member of Spinosauridae from the Enciso Group (uppermost Barremian-lower Aptian) from Igea (La Rioja, Spain) is here erected on the basis of axial, pelvic girdle and hindlimb elements that exhibit a unique combination of characters. *Riojavenatrix lacustris*, gen. et sp. nov., is one of the latest Iberian and also European spinosaurid taxa. It still retains the triangular pubic boot as the megalosaurids, and the medial condyle of the femur that shows a transitional stage between the anteroposteriorly oriented long axis of non-spinosaurid theropods and the posteromedially oriented long axis of Spinosauridae. The spinosaurid record of Iberia ranges from the late Hauterivian-early Barremian to the latest Barremian-early Aptian so far, and both the oldest and the youngest evidences come from the Cameros Basin, as the spinosaurid remains are especially abundant in the Barremian deposits. A review of the spinosaurid record has allowed to dismiss the presence of the genus *Baryonyx* in Iberia and, hence, only *Camarillasaurus*, *Iberospinus*, *Protathlitis*, *Riojavenatrix* gen. nov. and *Vallibonavenatrix* are considered to be present in the Early Cretaceous of Iberia. According to this study, *Riojavenatrix* would be one of the youngest baryonychines in the fossil record.

Abstract

A new member of Spinosauridae from the Enciso Group (uppermost Barremian-lower Aptian) from Igea (La Rioja, Spain) is here erected on the basis of axial, pelvic girdle and hindlimb elements that exhibit a unique combination of characters. *Riojavenatrix lacustris*, gen. et sp. nov., is one of the latest Iberian and also European spinosaurid taxa. It still retains the triangular pubic boot as the megalosaurids, and the medial condyle of the femur that shows a transitional stage between the anteroposteriorly oriented long axis of non-spinosaurid theropods and the posteromedially oriented long axis of Spinosauridae. The spinosaurid record of Iberia ranges from the late Hauterivian-early Barremian to the latest Barremian-early Aptian so far, and both the oldest and the youngest evidences come from the Cameros Basin, as the spinosaurid remains are especially abundant in the Barremian deposits. A review of the spinosaurid record has allowed to dismiss the presence of the genus *Baryonyx* in Iberia and, hence, only *Camarillasaurus*, *Iberospinus*, *Protathlitis*, *Riojavenatrix* gen. nov. and *Vallibonavenatrix* are considered to be present in the Early Cretaceous of Iberia. According to this study, *Riojavenatrix* would be one of the youngest baryonychines in the fossil record.

Keywords: Baryonychinae; Dinosaur; Early Cretaceous; Europe; Iberian Peninsula; Megalosauroidea; Spinosauridae; Theropoda.

INTRODUCTION

Spinosauridae comprises a bizarre group of large-sized theropods, characterized by elongated snouts, conidonty, robust forelimbs with a large manual ungual phalanx I, and tall neural spines forming a dorsal sail in some taxa (e.g., Charig & Milner, 1997; Sereno *et al.*, 1998; Holtz *et al.*, 2004; Bertin, 2010; Hendrickx *et al.*, 2015; Arden *et al.*, 2019). First erected on the basis of disarticulated elements from the Cenomanian of Egypt and the description of the enormous *Spinosaurus aegyptiacus* Stromer, 1915 (Stromer, 1915; Bertin, 2010), this tetanuran clade has been involved in great controversy. The morphology of the skull and teeth resembling those of crocodyliforms, and gut content with fish

scales suggest at least partially a piscivorous diet, but also feeding on dinosaurs and pterosaurs (e.g., Charig & Milner, 1997; Buffetaut *et al.*, 2004). Due to their feeding ecology, spinosaurid were at least partly dependent on aquatic habitats. It has also been proposed a predominant aquatic lifestyle for some spinosaurid taxa, such as *Baryonyx* Charig & Milner, 1986 and *Spinosaurus* even with a subaqueous foraging strategy (e.g., Ibrahim *et al.*, 2014, 2020; Beevor *et al.*, 2021; Fabbri *et al.*, 2022). Nevertheless, this still a highly debated topic (see e.g., Hone & Holtz, 2017, 2021; Heckeberg & Rauhut, 2020; Sereno *et al.*, 2022; Isasmendi *et al.*, 2023). Regardless, spinosaurids have usually been positively associated with coastal environments (Sales *et al.*, 2016).

Spinosaurids have been traditionally included within Megalosauroidea, as a sister group of megalosaurids (e.g., Sereno *et al.*, 1998; Rauhut, 2003; Allain *et al.*, 2012; Hone & Holtz, 2017; Malafaia *et al.*, 2020a). Spinosauridae comprises the subfamilies Baryonychinae and Spinosaurinae (Sereno *et al.*, 1998). Megalosauroidea was also considered paraphyletic in Rauhut & Pol (2019) and Spinosauridae would be early-branched within Carnosauria as sister taxa of Megalosauridae+Allosauroidea (Rauhut & Pol, 2019). Nevertheless, the more recent analysis carried out by Schade *et al.* (2023), based on a modified version of the Rauhut & Pol (2019) matrix, recovered again Megalosauroidea as a monophyletic clade, which included Spinosauridae within it. The division within Spinosauridae has also been questioned by Evers *et al.* (2015) and Sales & Schultz (2017). Indeed, Evers *et al.* (2015) did not find this traditional division strongly supported. According to the phylogenetic analyses carried out by Sales & Schultz (2017) baryonychines are recovered in a polytomy. Despite all the phylogenetic controversy, spinosaurids are always considered as a monophyletic group (e.g., Sereno *et al.*, 1998, 2022; Allain *et al.*, 2012; Carrano *et al.*, 2012; Sales & Schultz, 2017; Malafaia *et al.*, 2020a; Rauhut & Pol, 2019; Mateus & Estraviz-López, 2022; Schade *et al.*, 2023)

This clade of early-branching tetanurans has a wide geographic distribution, having been reported from Asian, European, North African and South American deposits that range from the Early Cretaceous to the Cenomanian (Bertin, 2010; Candeiro *et al.*, 2017; Hone & Holtz, 2017).

Nevertheless, spinosaurid fossil remains are rather uncommon, mostly consisting of isolated teeth and bone fragments (Holtz *et al.*, 2004; Bertin, 2010; Hone & Holtz, 2017). It is currently supposed that spinosaurids originated in Europe with at least two subsequent Early Cretaceous migrations to Africa (Milner, 2003; Barker *et al.*, 2021), but, recently three baryonychine teeth have been reported from the Berriasian–Valanginian deposits of the Feliz Deserto Formation of Brazil, suggesting a more complex scenario (Lacerda *et al.*, 2023). Hitherto, spinosaurids are particularly diverse in the Early Cretaceous European archipelago where they are represented by the genera *Baryonyx*, *Camarillasaurus* Sánchez-Hernández & Benton, 2014, *Ceratosuchops* Barker *et al.*, 2021, *Iberospinus* Mateus & Estraviz-López, 2022, *Protathlitis* Santos-Cubedo et al., 2023, *Riparovenator* Barker *et al.*, 2021 and *Vallibonavenatrix* Malafaia *et al.*, 2020a.

Besides *Camarillasaurus*, *Iberospinus, Protathlitis* and *Vallibonavenatrix*, other spinosaurid remains from the Iberian Peninsula have been assigned to baryonychines, specifically to the genus *Baryonyx* (Torcida *et al.*, 1997; Fuentes-Vidarte *et al.*, 2001; Buffetaut, 2007; Viera & Torres, 2013; Figueiredo *et al.*, 2015), but these attributions should be considered with caution due to the fragmentary nature of the specimens. Most of these spinosaurid remains consist of scattered bones or isolated teeth of both baryonychine and spinosaurine theropods (e.g., Torcida Fernández-Baldor *et al.*, 2003; Sánchez-Hernández *et al.*, 2007; Alonso & Canudo, 2016; Alonso *et al.*, 2017; Gasca *et al.*, 2018; Isasmendi *et al*., 2020, 2023). However, since new studies provide evidence for a more complex scenario in Iberia for spinosaurids, a revision of these fossils should be made based on the current record.

This paper is aimed to describe a partially articulated spinosaurid theropod from the Early Cretaceous Enciso Group of La Rioja (Spain). The specimen is here proposed as the holotype of a new theropod genus and species, *Riojavenatrix lacustris*, gen. et sp. nov., previously suggested to have baryonychine affinities (Malafaia *et al.*, 2018) or even assigned to the genus *Baryonyx* (Viera & Torres, 2013). The herein erected taxon contributes to a better understanding of the palaeobiodiversity of Spinosauridae in the Early Cretaceous of Europe and Gondwana. Furthermore, a review of the

current spinosaurid record is presented and the spinosaurid palaeobiodiversity of the Iberian Peninsula is analyzed.

GEOGRAPHICAL AND GEOLOGICAL SETTING

The partially articulated specimen (CPI1637–1648 and 1675–1677) was found in the locality of Igea (southeast of La Rioja, Spain), specifically at the Virgen del Villar-1 site (Fig. 1). This site is located southwest of the main town of Igea, near the Virgen del Villar hermitage (Fig. 1A).

Geologically, the Virgen del Villar-1 site is located in the northeastern part of the Cameros Basin. The Cameros Basin formed in the second rifting stage that took place during the Late Jurassic and Early Cretaceous in the Iberian Mesozoic Rift (Mas *et al.*, 2002). The deposits of the basin are mainly continental or coastal, reaching up to a thickness of 6,500 m in its depocentre, dating back to the Tithonian–early Aptian (Martín-Chivelet *et al.*, 2019 and references therein). These deposits have been traditionally divided into five lithostratigraphic groups (Tera, Oncala, Urbión, Enciso and Oliván groups) by Tischer (1966) or into eight depositional sequences (DS1–8) by Mas *et al.* (2002), where fluvial deposits derive laterally and upwardly into lacustrine deposits (Mas *et al.*, 1993, 2002; Hernán, 2018).

Two sub-basins can be differentiated in the Cameros Basin: Eastern Cameros and Western Cameros sub-basins (Mas *et al.*, 1993, 2002). The stratigraphic succession found at the Virgen del Villar-1 site is part of the DS 7 sequence of the Eastern Cameros sub-basin. Specifically, the fossil locality is situated in the Enciso Group (Fig. 1A), which constitutes the central sector of the Cameros Basin (Tischer, 1966; Hernán, 2018). This group is composed of mixed siliciclastic-carbonate deposits that exceed 2,000 m in thickness in the main depocentre of the basin (Clemente, 2010; Suarez-Gonzalez *et al.*, 2013), and its deposits have mainly been interpreted as a siliciclastic-influenced carbonate lacustrine and palustrine environment (Mas *et al.*, 1993, 2002, 2011), with also fluvial and deltaic episodes (Hernán, 2018).

Intense diagenesis and low-grade metamorphism (Casquet *et al.*, 1992) affected the sediments of the Enciso Group. Initially, by deep diagenesis conditions reached at burial depths between 5,000 and 6,000 m, and posteriorly, by a later (Albian) low-grade hydrothermal metamorphism, reaching temperatures between 300 and 350 °C, and burial pressures under 1–2 kbar respectively (Mata *et al.*, 2001; Del Rio *et al.*, 2009; Omodeo-Sal *et al.*, 2017 and references therein).

Regarding the age of the unit, several studies have proposed different chronological ranges (e.g., Alonso & Mas, 1993; Mas *et al.*, 1993; Martín-Closas & Alonso Millán, 1998; Schudack & Schudack, 2009; Casas *et al.*, 2009). Nonetheless, recent studies date the Enciso Group from the latest Barremian to the early Aptian, with most of the unit being early Aptian in age, with likely lowermost upper Aptian deposits in the uppermost part of the group (Suarez-Gonzalez *et al.*, 2013, 2015; Hernán, 2018).

MATERIAL AND METHODS

The described material (CPI1637–1648 and 1675–1677) consists of a vertebral element (fragment of a dorsal neural arch), pelvic girdle remains (left pubis, right ischium) and hindlimb bones (proximal end of a right femur, shaft and distal end of a left femur, proximal right tibia, left tibia, an almost complete left fibula, left astragalus, left calcaneum, metatarsal III, a possible metatarsal II, three left non-ungual pedal phalanges and left I-2 pedal phalanx) (Fig. 2). The left femur, tibia, astragalus and the calcaneum were found articulated. All the material likely belongs to the same individual, as they were recovered associated in the same part of the two square meters quarry, the consistent size of the fossils, and the lack of duplicated elements. The fossil material is housed at the Centro de Interpretación Paleontológica de La Rioja-CPI in Igea (La Rioja, Spain).

The studied material was examined and measured first-hand (all measurements are given in Supplementary Material 1). The following spinosaurid specimens were also directly examined or via photographs by one or more of the authors: *Baryonyx walkeri* Charig & Milner, 1986 (NHMUK VP R9951); *Camarillasaurus cirugedae* Sánchez-Hernández & Benton, 2014 (MPG-KPC1–46);

Iberospinus natarioi Mateus & Estraviz-López, 2022 (ML 1190); *Ichthyovenator laosensis* Allain *et al.*, 2012 (MDS-Savannakhet BK10-01–15); the proposed neotype of *Spinosaurus aegyptiacus* (FSAC-KK 11888; Ibrahim *et al.*, 2014); *Suchomimus tenerensis* Sereno *et al.*, 1998 (MNN GDF500); *Vallibonavenatrix cani* Malafaia *et al.*, 2020a (MSMCa-1–6, 9–15, 18–20, 22–24, 27–28, 32–33, 53–55). Besides the abovementioned taxa, two femora (CMP-3b/211 and CMP-MS-0/22) and a tibia (CMP-3c/188) published by Malafaia *et al.* (2018) were studied in person. Furthermore, comparisons with "*Spinosaurus* B" Stromer, 1934 (Nr. 1922 X 45) were made using the drawings in Stromer (1934). Only the specimen number is indicated when the observation was made first-hand by any of the authors. When the study was based on figures from previous works, the figures will be indicated and when previous authors made the observations, the references will only be included.

PHYLOGENETIC METHODOLOGY

We analysed the phylogenetic position of the new genus and species described here using a modified version of the matrix of Rauhut & Pol (2021), which, in turn, was previously modified from Wang *et al.* (2017). This character data matrix is a large dataset of theropod dinosaurs that is currently and continuously updated by the Mesozoic Tetrapod work group (main institutions in LMU and BSPG, Germany). The coding of the new taxon was added in this matrix, together with a review and re-score of other seven taxa (*Baryonyx, Camarillasaurus, Ichthyovenator, Sigilmassasaurus* Russell, 1996*, Spinosaurus, Suchomimus* and *Vallibonavenatrix*). For the analysis, *Sigilmassasaurus* and *Spinosaurus* genera have been distinguished as different OTUs (as proposed by Evers *et al.*, 2015). The neotype specimen proposed for *Spinosaurus* by Ibrahim *et al.* (2014) as well as the other elements attributed to the same genus have been coded within *Spinosaurus*. The original set of taxa from both used matrix have not been modified (no other taxa have been excluded or included). . The data matrix has 206 taxa and 774 characters, among which 118 are ordered multistate characters (see character list in Supplementary Material 2, nexus file of the matrix in Supplementary File S1).

The matrix was managed using Mesquite 3.01 (Maddison & Maddison, 2008) and imported into TNT 1.5 (Goloboff & Catalano, 2016). We performed a heuristic tree search in order to find most

parsimonious trees (MPTs), using the New Technology algorithms: sectorial searches and tree fusing, using the default settings for all of them. These algorithms were applied to new searched trees using the driven search to find the minimum length trees 100 times. Subsequently, we exposed the results to tree bisection reconnection (TBR) as a branch-swapping algorithm, saving 100 trees per replicate. The resulting MPTs were summarized using a strict consensus. The consistency index (CI) and the retention index (RI) were calculated using the *stats.run* script. The branch support was tested using the methodology proposed by Goloboff *et al.* (2008) to calculate Bremer support values and resampling methods such as Bootstrap and Jackknife (100 replicates, summarized as frequency differences).

Furthermore, to find unstable taxa, a reduced consensus tree was obtained using the IterPCR method (Pol & Escapa, 2009) with the *iterpcr.run* script. This methodology generated two outputs, the reduced consensus, a summary tree showing all the unstable and pruned taxa and its alternative position in the tree, and the analysis of the characters that contradicts some of the alternative positions and potential critical characters (see Supplementary Material 2). Two alternative approaches were carried out to evaluate unstable taxa: (1) Pruned trees method (Goloboff *et al.*, 2008), using the command *prunnelsen*; (2) the finding of the maximum agreement subtree (MAST), the largest subtree shared by all the MPT (Gordon, 1979, 1980).

In order to evaluate the alternative placement of pruned taxa in previous analyses, some constrained trees were defined forcing the unstable taxa in these alternative locations in the reduced consensus tree, using the command *force*=, and, posteriorly, making a search enforcing constraint (Goloboff *et al.*, 2008).

The appendicular characters have been mapped using Mesquite 3.01 (Maddison & Maddison, 2008) in the reduced consensus trees obtained by the IterPCR analysis, and also in the strict consensus tree in TNT, using the common map of characters analysis.

In addition to this phylogenetic analysis, the new taxon was also coded in a modified version of the matrix used by Mateus & Estraviz-López (2022) (Nexus file in Supplementary File S2), which, in

turn, was modified from Arden *et al.* (2019); Evers *et al.* (2015) and Carrano *et al.* (2012) and with skull characters added from Hendrickx *et al.* (2020). This matrix has a total of 534 characters and 24 taxa that have not been modified in this study. The aim of the phylogenetic analysis conducted in this study is to test the hypothesis of the position of *Riojavenatrix* obtained in the previous analysis using a matrix focused mainly on early-branching tetanurans. The methodology followed to run this analysis in TNT 1.5 was exactly the same as the one executed with the modified matrix from Rauhut & Pol (2021).

HISTOLOGY

Several fragmentary limb bones were selected for histological examination and prepared according to the usual methodology outlined by Chinsamy & Raath (1992), posteriorly developed in Lamm (2013). Nomenclature and definitions of bone microstructures are derived from Francillon-Vieillot *et al.* (1990).

INSTITUTIONAL ABBREVIATIONS.

AMNH, American Museum of Natural History, New York, USA; BSPG, Bayerische Staatssammlung für Paläontologie und Geologie, Munich, Germany; CPGP, Centro Português de Geo-História e Pré-História, Lisbon, Portugal; CPI, Centro de Interpretación Paleontológica de La Rioja, Igea, Spain; MDS-Savannakhet, Dinosaur Museum of Savannakhet, Savannakhet, Laos; FMNH, Field Museum of Natural History, Chicago, USA; FPMN, Fukui Prefectural Museum, Fukui, Japan; FSAC, Faculté des Sciences Aïn Chock, Casablanca, Morocco; IVPP, Institute of Vertebrate Paleontology and Paleoanthropology, Beijing, China; IWCMS, Dinosaur Isle Museum, Sandown, United Kingdom; LMU, Ludwig Maximillian University, Munich, Germany; MG, Museu Geológico, Lisbon, Portugal; MDS-Salas de los Infantes, Museo de Dinosaurios, Salas de los Infantes, Spain; MNHN, Muséum national d'Histoire naturelle, Paris, France; MNHN/UL, Museu Nacional de História Natural e da Ciência da Universidade de Lisboa, Lisbon, Portugal; ML, Museu da Lourinhã, Lourinhã, Portugal;

MNBH, Musée National Boubou Hama, Niamey, Republic of Niger; MNN, Musée National du Niger, Niamey, Niger; MPG, Museo Paleontológico de Galve, Galve, Spain; MSM, Museo Paleontológico Juan Cano Forner, Sant Mateu, Spain; NHMUK, Natural History Museum, London, UK; OUMNH, Oxford University Museum of Natural History, Oxford, UK; SHN, Sociedade de História Natural, Torres Vedras, Portugal; SM, Sirindhorn Museum, Department of Mineral Resources, Kalasin, Thailand; USNM, National Museum of Natural History, Smithsonian Institution, Washington, USA; WMN, LWL-Museum für Naturkunde, Münster, Germany; YPM, Yale Peabody Museum, New Haven, USA.

SYSTEMATIC PALEONTOLOGY

DINOSAURIA OWEN, 1842

THEROPODA MARSH, 1881

TETANURAE GAUTHIER, 1986

SPINOSAURIDAE STROMER, 1915

BARYONYCHINAE SERENO *ET AL.*, 1998

RIOJAVENATRIX GEN. NOV.

Etymology: Rioja (toponymy): in reference to La Rioja, the Spanish region where the holotype specimen was recovered, and *venatrix*: Latin for huntress.

Type and only species: As for the type species (see below)

Diagnosis: as for the type species (see below).

RIOJAVENATRIX LACUSTRIS SP. NOV.

Etymology: Latin for "related to a lake", which declines from the word "*lacus"* (lake).

Holotype: A partial skeleton of a single individual, including CPI 1637, left femur; CPI 1638, left tibia and astragalus; CPI 1639A–B, left fibula; CPI 1640, left metatarsal III; CPI 1641A–B, right

ischium; CPI 1642, right tibia; CPI 1643, right femur; CPI 1644, possible fragment of metatarsal II; CPI 1645, left phalanx III-1; CPI 1646, left phalanx III-3; CPI 1647, left phalanx I-2; CPI 1648, left phalanx IV-2 (or IV-3); CPI 1675A–B, left pubis; CPI 1676, left calcaneum; CPI 1677, fragment of a dorsal neural arch.

Type locality and horizon: Virgen del Villar-1 site, La Rioja, Spain; the Enciso Group is uppermost Barremian–lower Aptian (Suarez-Gonzalez *et al.*, 2013, 2015), but the type locality is most likely lower Aptian within the Enciso Group.

Diagnosis: A medium- to large-sized spinosaurid theropod with the following unique combination of characters within Spinosauridae: 1) a lateromedially thick and triangular pubic boot in distal view, with a straight posterolateral margin (similar to *Ichthyovenator*, but in *Itchthyovenator* this margin is concave, but absent in *Baryonyx*, *Suchomimus* and FSAC-KK 11888); 2) an anteroposteriorly expanded ischial boot with an anterodorsally oriented tip and an angular anterodistal surface (absent in *Ichthyovenator* and FSAC-KK 11888; similar to *Megalosaurus bucklandii*); 3) a narrow, restricted and relatively deep articular groove on the proximal surface of the femur, which is anteromedially-posterolaterally inclined (distinct to those of *Baryonyx* and *Suchomimus*); 4) a medial femoral condyle with the long axis only slightly posteromedially oriented (distinct to those in *Baryonyx*, "*Spinosaurus* B" (Nr. 1922 X 45), *Suchomimus* and FSAC-KK 11888); 5) presence of a vertical ridge on the medial margin of the ascending process of the astragalus (potential autapomophy, but it could also be a character in Spinosauridae, because no other spinosaurid astragalus has been described to date); 6) height of ascending process of the astragalus more than twice the height of astragalar body (potential autapomophy, but it could also be a character in Spinosauridae, because no other spinosaurid astragalus has been described to date); 7) presence of an anterior depression with a dorsally located foramen on the lateral surface of the calcaneum (autapomorphy; absent in other spinosaurids); and 8) absence of a longitudinal groove on the medial surface of phalanx I-2 (potential autapomophy, but it could also be a character in Spinosauridae or even in Megalosauroidea. As this element is not preserved in other spinosaurid or megalosauroid a synapomorphy cannot be excluded).

DESCRIPTION

AXIAL SKELETON

Dorsal vertebra (Fig. 3): This piece consists of the mid and posterior portions of the base of the neural arch, the bases of the transverse processes and the neural spine of a mid or posterior dorsal vertebra (CPI 1677). The neural arch does not preserve any of the zygapophyses. The thickness of the neural spine is constant across its anteroposterior length, but anteriorly, the interspinous ligament scar is present and slightly thickens the neural spine transversely (Fig. 3A). The right spinodiapophyseal fossa is smooth whereas the left one is more rugose. The transverse processes are horizontal in lateral view and slightly inclined dorsolaterally (Fig. 3B).

Anteriorly, the spinoprezygapophyseal laminae would have bounded a deep and dorsoventrally elongate spinoprezygapophyseal fossa, which is filled with matrix. This was inferred considering the distance between both laminae, the posterior extension of the fossa and the considerable missing anterior portion of the spine (Fig. 3A). On the posterior side, another fossa is present, interpreted here as the spinopostzygapophyseal fossa (Fig. 3C). This fossa is also dorsoventrally elongate and deep, delimited by the spinopostzygapophyseal laminae. Ventrally, these laminae merge to form the hyposphene (Fig. 3C). Underneath the left transverse process, a fragment of the posterior centrodiapophyseal lamina is centrally positioned, extending ventrally to the centrum (Fig. 3B). Posterior to this lamina, the postzygocentrodiapophyseal fossa is present on the right side of the neural arch (Fig. 3B). This fossa is also present on the left side, but it is less pronounced.

APPENDICULAR SKELETON

PELVIC GIRDLE

Pubis (Fig. 4A–J): Two fragments of the left pubis are preserved (CPI 1675A–B). The proximal fragment preserves the articular surface for the ischium, the surface of the acetabulum and the part of

the iliac articulation (Fig. 4A–E). The iliac articulation is broad, strongly rugose and somewhat convex in proximal view (Fig. 4E). Adjacent to the medial margin, an anteroposteriorly elongate concavity is present on this articular surface. However, this area is not well preserved and may be an artifact of abrasion. The iliac peduncle is not anteriorly complete, but it broadens towards the acetabular surface (Fig. 4E). The medial surface of the iliac peduncle is straight, becoming convex near the acetabular surface in proximal view. Posterior to the iliac articular facet, the acetabular surface is a small triangular concavity, which is located medially on the proximal surface, and posteromedially inclined (Fig. 4E). The ischial peduncle projects posteriorly and tappers posterodistally towards the ischial articulation (Fig. 4D). The ischial articulation is not completely preserved at the proximal end. It is triangular in posterior view and posteromedially directed (Fig. 4D). The obturator notch is distally opened, relatively small anteroposteriorly and subcircular (Fig. 4B–C).

The distal fragment of the left pubis (Fig. 4F–J) lacks part of the symphysis and the medial portion of the distal expansion (Fig. 4J). The shaft of the distal fragment is quite straight and shows a teardrop-shaped cross-section at the level of the symphysis. The pubic apron projects as a blade from the shaft (Fig. 4J). The symphysis is almost entirely missing, but the preserved distal part is medially projected. Furthermore, it is sigmoidal in medial view, with a large distal extension. Based on the breakage surface, its development and distalmost extension of the preserved apron, the pubic apron would have almost reached or slightly extended along the pubic boot (Fig. 4J). The pubis is slightly expanded anteriorly on its distal end, and it has a greater posterior projection (Fig. 4G, I). In distal view, the pubic boot is mediolaterally broad, especially at its center (Fig. 4H). Its anterior and medial surfaces are convex whereas the lateral surface is gently concave. The posterior process of the pubic boot tapers posteriorly, ending posteriorly in a tip. In distal view, the pubic boot is triangular in shape (Fig. 4H).

Ischium (Fig. 4K–T): The right ischium preserves its proximal end (including the iliac peduncle), part of the shaft and the ischial boot (CPI 1641A–B). Both lateral and medial surfaces of the iliac peduncle are convex (Fig. 4Q). At the level of the surface of the acetabulum, the medial surface is flat and the lateral one is slightly concave, whereas near the pubic peduncle, the medial surface becomes concave and the lateral surface convex (Fig. 4Q). In the posterior margin of the iliac peduncle, there is a dorsoventrally directed crest, forming a bulge near the dorsal margin. This bulge can be observed in medial and lateral views (Fig. 4L–N). Anterior to this crest, the medial surface shows some proximodistally oriented furrows.

The iliac peduncle is mediolaterally expanded, with an oval contour in proximal view (Fig. 4Q). Although it is abraded, the articular surface of the iliac peduncle is concave posteromedially. A protuberance is present at the center of the concavity bounded anteriorly and medially by a groove. This concavity is anterolaterally delimited by a transversely oriented edge (Fig. 4Q). The surface of the acetabulum bears a pronounced concavity that becomes shallower anteriorly. In proximal view, the acetabular surface has a medial crest, partially broken. This crest extends anteriorly from the anteromedial edge of the iliac articulation (Fig. 4Q).

The preserved cross-section of the ischium diaphysis is somewhat oval, with a rounded crest, posterolaterally directed, running longitudinally on the lateral surface of the shaft (Fig. 4O, R, S). The posterior surface of the diaphysis is concave proximally and flattens towards the ischial boot, becoming a crest at the boot (Fig. 4S). Both medial and anterior surfaces of the shaft are quite flat (Fig. 4O–P). The ischial boot, triangular in medial or lateral view, is not strongly anteroposterioly expanded, and exhibits an angular anterodistal surface (Fig. 4P, R). The posterior half of the lateral surface is convex whereas the anterior half shows a concavity caused by the anterior process of the ischial boot (Fig. 4R). This anterior process is connected to the diaphysis by a blade that becomes gradually less prominent proximally (Fig. 4R). The blade is laterally inclined distally and becomes vertical proximally. The medial surface of the ischial boot is flat and shows some longitudinal

striations that run proximally to the shaft (Fig. 4P). In distal view, the ischial boot shows a triangular outline due to the tapering of the anterior process (Fig. 4T).

HINDLIMB

Femur (Fig. 5): The right femur only preserves its proximal end (CPI 1643), and the left femur consists of most of the diaphysis and the distal articular end (CPI 1637). The femoral head is gently convex and subcircular in medial view (Fig. 5D). Its proximodistal axis is slightly longer than the anteroposterior one. The femoral head is medially oriented and anteromedially directed at an angle of about 20º (Fig. 5J). The proximal surface of the femur is posterolaterally inclined. There is an anteroproximally inclined groove (i.e., the oblique ligament groove) on the posterior surface (Fig. 5C). This groove separates the femoral head from the shaft; therefore, the latter is well offset medially. Medial to this groove, the posterior lip of the fermoral head is well-developed and slightly extends beyond the posterior surface of the head (Fig. 5C, J). The femoral head has a concave ventral surface. This surface becomes broader anteriorly, making the femoral head overhang the medial surface of the femoral diaphysis (Fig. 5A, C). On the anterior side of the femoral head, there is an oblique ridge that extends from the femoral head to the proximal end of the diaphysis (Fig. 5A). In proximal view, a deep, broad and oblique articular groove can be noticed. This is more pronounced anteromedially and becomes shallower and narrower posterolaterally. In the same view, the femoral head is laterally confluent with the greater trochanter, which is incomplete and narrower than the head (Fig. 5J).

The left femur lacks the proximal end and the diaphysis proximal to the fourth trochanter. The preserved length of the left femur measures c. 515 mm. The shaft of the femur is rather straight in anterior and posterior views, but it is anteriorly bowed in lateral and medial views (Fig. 5E–H). The diaphysis is oval in cross-section, the mediolateral axis being larger than the anteroposterior one, with a maximum circumference of 322 mm. The anterior surface of the shaft is convex and slightly pinched in the middle (Fig. 5E). The pinch extends 190 mm distal from the proximal fracture. Medial and lateral to this pinch, the surface becomes flat. The lateral surface is convex and becomes flat next to the distal expansion of the bone (Fig. 5F). The medial surface is also convex but leads to a shallow

and large concavity, which is located posterior to the medial epicondyle and extends until half of the medial condyle (Fig. 5H). The posterior surface of the femoral shaft is flat and faces posterolaterally (Fig. 5G).

The fourth trochanter is located posteromedially in the proximal part of the preserved shaft. Only its most distal end is preserved, consisting of a well-developed and prominent longitudinal crest that becomes broader proximally (Fig. 5G). Medially, there is a shallow and smooth groove; and laterally, there is a shallow, smooth and broad concavity, which is excavated in the posterior surface of the diaphysis in lateral view.

The distal end of the femur is slightly more medially than laterally expanded in posterior view (Fig. 5G). The medial epicondyle or medial distal crest is found on the mediodistal surface. This medial epicondyle is rounded, low and not well developed (Fig. 5E). On the anterior surface of the medial epicondyle, the attachment for the *M. femorotibialis externus* is a small rugose patch. The extensor groove is broad and slightly V-shaped in distal view (Fig. 5I) and gets even shallower and broader proximally (Fig. 5E). The flexor groove is rather broad, deep and U-shaped in distal view (Fig. 5I). The flexor groove is bounded by two ridges medially and laterally, proximal to the condyles (Fig. 5G). The medial ridge runs vertically from the proximal margin of the medial condyle whereas the lateral ridge is more prominent and oblique, originating at the proximal end of the tibiofibular crest. The medial crest merges with the shaft proximally.

The anterior surface of the lateral condyle is rounded. The medial condyle is slightly more flattened and anterolaterally oriented in the anterior surface (Fig. 5E). In the distal end, the condyles are robust, being wide mediolaterally. Both medial and lateral condyles project distally almost equally in anterior view (Fig. 5E). In the same view, the lateral condyle projects distally and slightly laterally, whereas the medial condyle is solely distally projected. The medial condyle is teardrop-shaped in posterior view (Fig. 5G). In distal view, the lateral condyle is rounded and the medial one is more elliptical with the long axis slightly posteromedially oriented (Fig. 5I). The distal condyles are not separated by an anteroposterior pronounced groove in the distal surface, but there is a central shallow groove

that connects to the tibiofibular crest (Fig. 5I). The tibiofibular crest is broad and positioned on the posterior surface of the lateral condyle (Fig. 5G, I). In posterior view, the crista tibiofibularis is teardrop-shaped and oblique in respect to the long axis of the lateral condyle (Fig. 5G). The tibiofibular crest is somewhat trapezoidal in distal view. This is laterally bounded by a broader groove and, medially, a narrow and deep groove separates the crest from the distal margin of the condyle or the flexor groove. Between both grooves, there is a posterolaterally elevated ridge in distal view (Fig. 5I).

Tibia (Figs. 6A–J and 7A–E): The right tibia (CPI 1642) only preserves its proximal portion (Fig. 6A–D, I). The left tibia (CPI 1638) is complete, including the articulated astragalus (Figs. 6E–J and 7A–E). The right tibia lacks the cnemial crest and the medial condyle. However, the lateral condyle and the proximal end of the fibular crest are well preserved.

The left tibia shows many furrows on the medial surface close to the proximal end. Furthermore, these are also present on the anterior margin of the medial malleolus. The shaft of the left tibia is straight and quite robust, with a length of c. 810 mm (Fig. 6E–H). The cross-section of the tibia diaphysis is oval, where the mediolateral axis is the largest. At mid-shaft, the diaphysis narrows laterally and wides medially. In lateral view, the anterior surface of the tibia is concave proximally, becoming convex distally. The posterior surface is rather straight close to the proximal end and concave distally. The anterior surface is flat and the posterior surface is gently convex along the whole shaft. The lateral surface is convex, whilst the medial margin is flat proximally and becomes concave at mid-shaft.

The cnemial crest of the left tibia is rounded (Fig. 6E–F). Dorsally, it expands mediolaterally and flexes laterally in anterior view. The cnemial crest projects from the anterior surface of the diaphysis beyond the proximal articular surface of the tibia (Fig. 6E–F). The lateral surface of the cnemial crest bears a longitudinal tuberosity near its anteroposterior corner (Fig. 6F, J). In proximal view, the lateral condyles are offset from the cnemial crest by a poorly-developed *incisura tibialis* (Fig. 6I–J). The

lateral condyles are large, rounded and broad. The preserved portions of both medial condyles suggest they were also large. There is no process extending anterolaterally from the lateral condyle in any tibia, but there is a notch present between the medial and lateral condyles in the right tibia (Fig. 6I). In proximal view, the posterior outline of the left tibia is nearly straight due to the lack of the medial condyle, whereas the medial surfaces are smoothly convex in both tibiae.

The fibular flange is a low longitudinal crest with a slightly broadened base (Fig. 6E–G). It is situated proximally on the lateral surface of the diaphysis, but it is distally located to the proximal end of the tibia. The outline of the base of the fibular crest is oval, but narrow, in lateral view (Fig. 6F). This is separated from the proximally located lateral process associated to the fibular crest. In the right tibia, the proximal end of the lateral process associated to the fibular crest also reaches the proximal end of the tibia (Fig. 6B, E–G, H). These processes are rounded and proximodistally oriented (Fig. 6B and F).

The distal end of the tibia is expanded mediolaterally, being anteroposteriorly narrower. Both the lateral and medial malleoli extend somewhat equally distally, with the lateral malleolus being larger and slightly more distally projected than the medial one (Figs. 6E, G and 7A, C). This makes the distal surface almost horizontal with c. 15º respect to the horizontal or c. 75º with respect to the long axis of the tibial shaft. The lateral malleolus is rounded and the medial one is more angled in posterior view (Figs. 6G and 7C). In medial view, the medial malleolus shows a flat surface bounded posteriorly by a longitudinal ridge, which is mediodistally inclined (Figs. 6G–H and 7C–D). The medial malleolus is transversely wider and more robust than the lateral one. The facet for the fibula shows longitudinal furrows and occupies a large portion of the anterior surface of the lateral malleolus (Figs. 6E–F and 7A–B). The astragalar facet of the tibia is high (c. 150 mm), broad, triangular and occupies more than half of the distal end of the anterior surface of the tibia (Figs. 6E and 7A). This facet is delimited proximomedially by the supraastragalar buttress. The latter is developed as a well-developed and bluntly rounded ridge. It originates mediodistally and it is almost vertical basally,

becoming a low oblique ridge proximally. The supraastragalar buttress is more pronounced distally and gradually fades proximolaterally (Figs. 6E and 7A).

Fibula (Fig. 6K–T): The left fibula (CPI 1639A–B) is almost complete but lacks part of the distal diaphysis. The fibula is a slender bone with a rather thin shaft, with an estimated length of 750 mm. The proximal end is strongly anteroposteriorly and also slightly mediolaterally expanded. Furthermore, the fibula is deformed, displaying an S-like shape at about 340 mm from its proximal end. Below the S-like deformation, the shaft of the fibula is somewhat twisted, a feature that may be associated with the deformation (Fig. 6K–N).

The proximal end of the fibula is more posteriorly than anteriorly expanded (Fig. 6L, N). The posterior margin of the proximal fibula gets thinner posteriorly to form a thin blade-shaped margin (Fig. 6O). This margin is more rounded than the anterior one in medial view, which is more acute in lateral view (Fig. 6L, N). The proximal margin is slightly concave at the level of the medial fossa and becomes convex near the anterior and posterior margins in lateral view (Fig. 6L, N). In proximal view, the proximal margin of the fibula is comma-shaped, with the anterior margin being wider than the posterior one (Fig. 6O).

The medial fossa reaches the proximal margin and occupies half of the expansion of the proximal end of the tibia. It is shallow, inverted teardrop-shaped and centrally positioned in medial view (Fig. 6N). Anteriorly, the medial fossa is bounded by an elevated edge, which creates the anterior margin of the proximal end and broadens proximally. The posterior margin of the medial fossa is posteriorly opened (Fig. 6N). Below the medial fossa, the medial surface is planar. In the shaft, a posteromedially located low ridge runs ventrally and becomes oblique below the iliofibularis tubercle, bounding an anterior groove on the medial surface. At the level of this tubercle, a shallow depression can be noticed on the medial surface of the shaft (Fig. 6N). Below the oblique ridge, a proximally well developed groove is present which extends parallel to the diaphysis distally. The posterior edge of this groove consists

of a medially raised edge. Distally, the groove fades at the distal end of the preserved shaft when the diaphysis expands (Fig. 6N).

At the proximal expansion of the fibula, the lateral surface is convex anteriorly, becoming almost flat in the middle of the lateral side, and again slightly convex posteriorly (Fig. 6L). Some longitudinal furrows are present on the anterolateral surface of the fibula. Posteriorly, the proximolateral surface of the fibula has a longitudinal and vertically oriented depression. Another broader, but slightly shallower depression is present on the anterolateral surface, at the same level as the posterior one (Fig. 6L). The fibular diaphysis has a strongly convex lateral surface, but it is more planar at the level of the iliofibularis tubercle.

The insertion for the iliofibularis muscle is located on the anterior margin of the fibular shaft, approximately at one third from the proximal surface (Fig. 6K–L, N). It is low and rugose in anterior view, and formed by two protuberances, which are laterally bounded by a longitudinal, shallow and rugose groove (Fig. 6K–L, N).

The distal end is expanded anteroposteriorly and transversely. At the beginning of the distal expansion, both anterior and posterior edges are sharp. Distally, the anterior part is rounded (Fig. 6P) whereas the posterior margin is sharp edged and slightly laterally inclined (Fig. 6R). The medial surface for the articulation with the tibia is proximally flat (Fig. 6S). However, in distal view, the anterior portion of the medial surface appears convex, becoming concave posteriorly (Fig. 6T). On the lateral surface of the distal expansion, an oblique ridge starts anteroproximally and runs posterodistally down to the ventral end (Fig. 6Q). Posteroproximally, overlaying this ridge, there is a shallow and broad depression. The distal outline of the fibula is teardrop-shaped. This surface shows a depression anteromedially and becomes convex posteriorly (Fig. 6T).

Astragalus (Figs. 6E–H and 7A–E): The left astragalus is almost complete (CPI 1638), only lacking part of the anterodistal margin of the medial condyle of the astragalar body. The astragalus is L-shaped in lateral view, with a relatively tall ascending process (Figs. 6E–F and 7A–B). The astragalus

measures 155 mm in height and 122 mm mediolaterally. In anterior view, the astragalar body shows an hourglass shape, with concave distal and proximal surfaces (Figs. 6E and 7A). However, the distal concavity is broader and less pronounced than the dorsal one. In distal view, the astragalar body is rectangular (Fig. 7E). The medial condyle of the astragalus is anteroposteriorly expanded. There is a shallow distal groove, becoming broader and slightly deeper laterally. The groove is bounded anteriorly by a parallel low crest that is slightly more prominent laterally and almost reaches the astragalus-calcaneum contact (Fig. 7E). In anterior view, there is another groove, horizontal and shallow, developed between the condyles, at mid-height of the astragalar body (Fig. 7A). This groove has its maximum depth medially, gradually gets shallower laterally, and extends until the lateral rim. There is a bulge on the groove. Between the astragalar body and the ascending process, there is a depression, and hence, the ascending process is offset from the astragalar body (Fig. 7B). This depression is broader and more marked laterally, showing a triangular shape in proximal view. The facet for the fibula is not preserved. The medial side of the posterior margin of the astragalar body is more proximally projected than the lateral side (Fig. 7C). This posterior margin is gently convex over most of its extension, but it laterally becomes shorter and slightly concave. The astragalar body is smooth on most of its anterior surface. Nonetheless, the area that articulates with the calcaneum is rugose.

The medial condyle is more anteriorly projected than the lateral one in ventral view and, hence, the astragalus is narrower laterally (Fig. 7E). Besides the anteroposterior expansion of the astragalar body, the distal condyles are anterodistally oriented. The distal condyles of the astragalus are anteroposteriorly rounded (Fig. 7E).

The ascending process of the astragalus is laminar, triangular and proximolaterally oriented (Fig. 7A). The height of the ascending process is twice the height of the astragalar body, measuring the former c. 103 mm and the latter 52 mm. The ascending process is slightly laterally located, and it does not reach the lateral margin of the astragalar body (Fig. 7A). It arises at around one-fifth from the medial margin of the astragalar body. The process is transversely broad, with its base extending

mediolaterally about 65% of the transverse width of the astragalar body. The medial margin of the ascending process shows a well-defined ridge that is perpendicular to the mediolateral axis of the astragalar body and arises from the anterodorsal surface of the astragalar body (Fig. 7A). This ridge is parallel to the ventral part of the astragalar buttress of the tibia. The ridge fades where the ascending process tilts laterally at an angle of 40–45º with respect to the long axis of the tibia. Proximally, this margin gradually becomes more transversely oriented. The lateral margin of the ascending process is rather straight and vertical (Fig. 7A). The proximal end of the ascending process is placed at three-quarters of the transverse width of the astragalar body from the medial side. The ascending process does not contact the supraastragalar buttress (Fig. 7A).

Calcaneum (Fig. 7F–K): The left calcaneum (CPI 1676) is complete, with a height of 63 mm. Its anteroposterior width measures 72 mm whereas its mediolateral width is 29 mm in length. The contact of the calcaneum with the astragalus is slightly sinuous and the tibia overlaps the calcaneum. The calcaneum is reniform anteriorly and laterally (Fig. 7H–I). In lateral view, the anteroproximal margin is more proximally elevated than the posteroproximal margin (Fig. 7I). The proximal rim is concave for the articulation with the fibula and the proximal articular surface is proximally directed. The articulation for the distal end of the fibula is well-developed (Fig. 7F). The distal profile is strongly convex in lateral view (Fig. 7I). In proximal view, the calcaneum is anteriorly broad, narrowing posteriorly, with a sharp edge that is posterolaterally oriented (Fig. 7F). This edge broadens distally and has a crescent shape in order to accommodate the lateral malleolus of the tibia (Fig. 7J). The lateral surface has a broad vertical groove and another anteriorly located depression. The latter is as deep as the groove, triangular and bears a foramen at its proximalmost point (Fig. 7I). Between the groove and the depression, a triangular convexity is present. The medial surface of the calcaneum shows a concave facet for the lateral malleolus and an anteriorly located groove to articulate the lateral condyle of the astragalus. The latter one is posteriorly inclined and parallel to the anterior margin of the calcaneum (Fig. 7K).

Metatarsal III (Fig. 8A–F): The left metatarsal III is complete (CPI 1640). The diaphysis is straight, measuring 364 mm proximodistally, and with a subrectangular cross-section at mid-shaft (Fig. 8C–E). Its borders are rounded, except for the medial surface that is planar. Its proximal end is anterodorsally and posteroventrally expanded, especially posteroventrally projected in lateral view (Fig. 8C, E).

In proximal view, metatarsal III has an hourglass-shaped outline, the anterodorsal part of which is more lateromedially expanded than the posteroventral one (Fig. 8F). The articular surface for metatarsal II is proximally located in the medial surface of metatarsal III (Fig. 8E). It is concave, densely striated and reaches the middle of the diaphysis. The articular surface for metatarsal IV is posteroventrally concave and convex anterodorsally close to the proximal end of metatarsal III (Fig. 8C). This surface is also striated like in the articulation for metatarsal II. The medial articular surface is anterodorsally and posteroventrally bounded by two elevated edges that fade distally. The posteroventral edge is more pronounced than the anterodorsal one. On the anterodorsal surface, there is a marked scar (Fig. 8B). Another scar is also located on the posteroventral surface, below the proximal expansion (Fig. 8D).

The distal condyle is posteroventrally divided by a shallow groove (Fig. 8A). On the anterodorsal surface, there is no marked hyperextensor pit; however, a subtle depression is present adjacent to the condyle (Fig. 8A–B). The distal condyle is subrectangular in distal view, with the medial side being anterodorsally and posterooventrally larger than the lateral side (Fig. 8A). The medial collateral ligament pit is much deeper and larger than the lateral one. Both of them are suboval (Fig. 8C, E).

Phalanx I-2 (Fig. 8G–K): CPI 1647 was interpreted as the ungual phalanx of digit I based on the small size of the element and its significant curvature which measures 63 mm proximodistally. This (left) phalanx is complete . It is long, narrow, distally pointed and strongly arched in lateral and medial

views (Fig. 8H, J). The phalanx I-2 is triangular in cross-section, but has an oval articular surface in proximal view (Fig. 8K). The articular surface for the articulation of I-1 phalanx is concave. This surface is slightly pointed dorsally in proximal view and the proximodistal lip is not well-developed. Ventrally, this surface is rounded. The flexor tuberosity, placed on the ventral side of the articular surface, is not very pronounced, but it is more developed than the lip (Fig. 8K). Both medial and lateral surfaces are convex proximally, but the lateral surface is slightly flatter (Fig. 8H, J). The dorsal surface of phalanx I-2 is convex and the ventral side is comparably flatter (Fig. 8G, I). There are no ventral or flexor fossae. Both medial and lateral margins are softly convex and, hence, this phalanx is quite symmetrical. Only the lateral surface bears a longitudinal groove. This is well developed and faces at about two-thirds proximally, becoming progressively shallower (Fig. 8H).

Phalanx III-1 (Fig. 8L–Q): CPI 1645 is interpreted as a proximal phalanx due to it lacking a proximal keel. Furthermore, it can be confidently assigned to digit III based on the rather symmetrical distal condyles and not as asymmetrical proximal articular surface. The left phalanx III-1 is virtually complete, measuring 118 mm in length, with the flexor tubercle partially eroded and lacking the ventral part of the medial condyle. The height and width of the phalanx change proximodistally, being higher proximally. Between both articular surfaces, the neck constricts the phalanx, especially ventrally, so the phalanx is wider than tall at mid-shaft (Fig. 8N, Q).

The dorsal margin is smooth, gently convex, becoming flat and inclined distally. Above the proximal margin of the collateral ligament pits, is the extensor fossa (Fig. 8M). It is quite deep, oval with the longest axis transversely directed. The ventral surface is also softly mediolaterally convex, but proximodistally concave in lateral and medial views (Fig. 8M, P, Q). Proximally, there is a proximolaterally oriented oblique groove that separates the flexor tubercle into two processes. The proximal articular surface is devoid of any keel separating the articular facets. This surface is weakly concave and subcircular, with a pronounced, medially inclined proximodorsal lip. This surface is partially deformed (Fig. 8O).

Close to the proximal end, there is a proximoventral fossa on both medial and lateral sides (Fig. 8N, Q). These are rugose and roughly triangular. Distally, the lateral collateral ligament pit is subcircular and deeper than the medial one. The medial collateral ligament pit extends more proximally and is oval (Fig. 8N, Q).

Both condyles are equally developed (Fig. 8L). The long axis of the lateral condyle is slightly laterally inclined and the medial condyle is somewhat medially inclined. The lateral condyle is slightly more dorsally and ventrally projected, whereas the medial condyle is slightly more distally projected (Fig. 8M, P). The condyles are separated by a shallow intercondylar sulcus. In distal view, the condyles are mediolaterally expanded on the ventral surface. In ventral view, the lateral condyle ends more abruptly proximally or, at least, it is more pronounced than the medial one (Fig. 8P).

Phalanx III-3 (Fig. 8R–W): CPI 1646 can be confidently attributed to digit III because symmetry of the distal condyles and the proximal articular surface. The specimen is not a proximal phalanx because it presents a keel on the proximal surface and is here identified as a III-3 based on the position of the collateral ligament pits, which are dorsally displaced, and the lack of a dorsal extensor fossa. The left phalanx III-3 is complete and almost symmetrical axially. Compared to phalanx III-1, this is smaller, measuring 67 mm in length, but stouter and proportionally transversely broader. This is taller and wider proximal and distally. The neck of phalanx III-3 especially constricts the pedal element.

The dorsal surface is convex, but concave in lateral or medial view (Fig. 8T, W). There is not a extensor fossa on the dorsal surface of this phalanx (Fig. 8S). The ventral surface is flat, but it is also concave in medial or lateral view (Fig. 8T, W). Two rounded and considerably broad proximoventral crests are present and they are bounded medial and laterally by a rugose area (Fig. 8T, V, W). Proximally and centrally positioned on the ventral surface, there is a process. The proximal end of the process is missing, but the preserved part is broad, rounded and proximodistally oriented. The proximal articular surface is triangular in outline in proximal view, with a well-developed and

centered proximodorsal lip (Fig. 8U). A vertical median keel separates the lateral and medial articular facets. Both articular facets are equally developed and subsymmetrical.

In medial and lateral views, the proximoventrally located fossae are less developed in III-3 phalanx than in III-1 (Fig. 8T, W). On the medial side, the fossa is restricted to a triangular rugose patch. On the lateral margin, this fossa is oval and very small. Both collateral ligament pits are more dorsally placed, as compared to phalanx III-1. These pits are quite deep, subcircular to oval and almost equally developed.

The distal condyles are not symmetrical. The medial condyle is more dorsoventrally developed compared to the lateral one (Fig. 8R). The long axis of the lateral condyle is laterally oriented and it is medially directed in the medial condyle. In ventral view, the lateral condyle ends more abruptly proximally (Fig. 8V).

Phalanx IV-2 (or IV-3) (Fig. 8X–AB): It is a proximal fragment of a left pedal phalanx IV-2 or IV-3 (CPI 1648). This identification is based on high asymmetry of the proximal articular surface, which indicates it would be from the digit IV. Furthermore, the presence of a keel on the proximal articular surface and the relative large size of the element suggest it would not be the distalmost non-ungual phalanx of digit IV. This fragment broadens and increases its height proximally. The neck of the phalanx would also contract the bone (Fig. 8X, Y, AA, AB). At this level, it is triangular in cross-section with rounded margins.

The dorsal surface of this phalanx is convex, but it is concave in lateral or medial view (Fig. 8Y, AB). The preserved ventral surface shows a smooth fossa, which is bounded by two proximoventral ridges (Fig. 8AA). The lateral ridge is broader than the medial one. Close to the proximal rim, there is a rugose surface. At the proximal rim, there is a centered proximal process. In proximal view, the proximal articular surface is triangular and bears a median keel that separates both articular surfaces for the condyles (Fig. 8Z). The proximodorsal lip is very pronounced and medially directed. The lateral articular facet is smaller but deeper than the medial one. The lateral articular facet is triangular

(almost right triangular) in proximal view, and the medial one is oval. Dorsal to the proximoventral ridges, there are no proximoventral fossae. In this area, a triangular rugose surface is present on both sides (Fig. 8Y, AB).

PHYLOGENETIC RESULTS

MATRIX RAUHUT & POL (2021)

The phylogenetic analysis resulted in 10000 most parsimonious trees with a length of 5386 steps (CI: 0.180; RI: 0.614). The strict consensus (Fig. S1 in Supplementary Material 2) shows a rather well-resolved topology of general non-tetanuran relationships, including the monophyletic Ceratosauria. Although Tetanurae is also solved as monophyletic, the non-Coelurosauria tetanuran clades are poorly solved, with more completely known taxa as *Allosaurus*, *Asfaltovenator, Concavenator or Spinosaurus* placed within a large and complex polytomy with several taxa and clades of different degrees of instability within Tetanurae. Piatnitzkysauridae, megalosaurines (*Megalosaurus, Torvosaurus gurneyi, Torvosaurus tanneri* and *Wiehenvenator*); some megaraptorans; metriacanthosaurids; some carcharodontosaurids; tyrannosaurids and Coelurosauria are found as monophyletic groups within this large polytomy in Tetanurae. However, *Riojavenatrix* is located in this high-grade polytomy, early-branched with the majority of other members of Carnosauria (Allosauridae + Megalosauridae clade, currently redefined by Rauhut & Pol, 2021), as well as all spinosaurids.

Therefore, we focus on the outcomes of the iterative PCR and other methodologies of pruning in order to analyse the unstable taxa that affect this complex polytomy and to know if *Riojavenatrix* is one of these unstable taxa, to evaluate the causes of this uncertainty and to use this information to find the possible solutions.

The reduced strict consensus from iterPCR (Fig. 9) was finished after a total of 7 iterations. A total of 27 terminal taxa and one clade (megaraptorans) was pruned as unstable taxa, where *Riojavenatrix*

was included (pruned in iteration 4). In the interaction 3, several clades within the tetanuran polytomy were established as monophyletic, as Megalosauroidea. *Riojavenatrix* was branched in a polytomy with other spinosaurids within Megalosauroidea. In the final reduced consensus, for the interrelationships of spinosaurids, *Camarillasaurus, Irritator, Riojavenatrix, Sigilmassasaurus* and *Vallibonavenatrix* (Fig. 9) were found as unstable taxa in the MPTs due to the fragmentary nature of the majority members of Spinosauridae, with a many characters coding as missing data. With these taxa removed, Spinosauridae is split into two groups, Baryonychinae (*Baryonyx* + *Suchomimus*) and Spinosaurinae (*Ichthyovenator* + *Spinosaurus*). In order to evaluate the position of *Riojavenatrix*, a reduced consensus with manual pruning (command *punnelsen*) of the unstable spinosaurids, except *Riojavenatrix,* was carried out. The results (Fig. S3 in Supplementary Material 2) show that the polytomy is still a high-degree one and that spinosaurids still remain located within this polytomy. The alternative positions of the pruned taxa (*Camarillasaurus, Irritator, Sigilmassasaurus* and *Vallibonavenatrix*) are: (1) all of them as early-branched tetanurans; (2) all of them in a dichotomy with *Riojavenatrix*; (3) *Irritator* related to *Suchomimus* in a dichotomy; (4) *Irritator* located in a dichotomy with *Baryonyx*; (5) *Vallibonavenatrix* related to *Leshansaurus* in a dichotomy.

Using the *prunnelsen*, for improvement the establishment of clades of the node of Tetanurae (node 226 in TNT, considered as a polytomy of degree 38) and calculating prunings until 3 taxa, we can see that the most common spinosaurids pruned are *Irritator*, *Riojavenatrix* and *Vallibonavenatrix*. These are the same results as in iterPCR methodology, where these taxa were also considered as unstable taxa. The manually pruning of these taxa shows a reduced strict consensus with a monophyly of *Baryonyx* and *Suchomimus*, where these three pruned taxa have several alternative positions. *Riojavenatrix* could be located as an early-branched baryonychine or in a dichotomy with *Suchomimus* within Baryonychinae (Fig. S2 in Supplementary Material 2). The agreement subtree was not obtained by TNT due to the numerous alternative results when dichotomies are forced.

The alternative position of the unstable taxa in spinosaurids (*Irritator*, *Riojavenatrix* and *Vallibonavenatrix*), based on the results in the pruning methodology of TNT, were forced in several

constraints (see Supplementary Material 2). Constraint obtained by forcing *Riojavenatrix* as a baryonychinae is rather well supported, requiring only three additional steps (length of 5389, 200 trees retained). When forcing the position of *Riojavenatrix* within Baryonychinae, it is mostly resolved the high-degree polytomy, and it is recovered most "traditional" monophyletic groups within Tetanurae. One of these recovered groups as monophyly is Spinosauridae, whose monophyly is also recovered in the reduced consensus tree from the iterPCR (Fig. 9). However, apart from the forced monophyly of baryonychines with *Riojavenatrix*, other monophyletic groups within Spinosauridae are not established. In this result, the sister taxa of Spinosauridae is a dichotomic group of *Lourinhanosaurus* and *Monolophosaurus*. When forcing *Riojavenatrix* and *Suchomimus* together, the support has a similar result, also requiring only three additional steps (length of 5389, 200 trees retained). However, the position of this forced group has numerous alternative positions within Spinosauridae, probably for the splitting up of Baryonychinae.

The Bremer support analysis (all taxa included) show many clades with minimal support. Tetanurae, including the high-degree polytomy, has a Bremer support of 1. However, monophyletic groups such as Megalosauridae have high values of Bremer support (3 and 5). The results of support for Jackknife and Bootstrap analyses show that most of the groups have values below 50%. Spinosaurids are all grouped here together, but with a low Jackknife support value of 2. In Bootstrap, *Baryonyx, Irritator* and *Suchomimus* are grouped together with a support value of 4, but the other spinosaurids are branched in the polytomy of tetanurans, which has a Bootstrap value of 27 (see Supplementary Material 2).

As was found out by the iterPCR and other methods of pruning, there are numerous unstable taxa in the matrix. This taxon instability could be one of the reasons for these low measures of support. Therefore, the position of all the unstable spinosaurids pruned in the reduced consensus by the iterPCR (see above) was ignored during another round of the Jackknife and Bootstrap support analyses. The results reveal that Spinosauridae improved its support values (Jackknife values: 20 for Spinosauridae, 70 for Baryonychinae, 37 for Spinosaurinae; Bootstrap values: 8 for Spinosauridae,

52 for Baryonychinae, 23 for Spinosaurinae) (see Supplementary Material 2).Appendicular skeleton is rarely described in spinosaurids so far. The placement of *Riojavenatrix* within Spinosauridae in the phylogenetic results allows to discuss those appendicular characters that may diagnose Spinosauridae and support the placement of *Riojavenatrix* within the clade. For that, appendicular characters have been mapped on the reduced consensus trees using Mesquite and also in the strict consensus in TNT.

Riojavenatrix shares the following characters with megalosauroids within Carnosauria: faint scar of the *M. femorotibialis externus* (ch. 692; shared with *Cryolophosaurus* and some early-branched theropods); weak medial epicondyle in femur (ch. 694; plesiomorphic condition present in *Herrerasaurus*, *Dilophosaurus wetherilli;* some coelophysoids, and some coelurosaurs); metatarsals less than 50% of tibial length (ch. 746; present in *Afrovenator, Eustreptospondylus, Riojavenatrix* and *Spinosaurus*; and some other theropods outside megalosauroids).

After mapping appendicular characters of *Riojavenatrix* on the reduced consensus trees and the previous anatomical comparison, the following unique combination of characters supports its placement as spinosaurid: the pubic apron extended from middle of the pubic shaft (Ch. 646; present also in *Ichthyovenator*; but absent in *Spinosaurus* and unknown in *Baryonyx* and *Suchomimus*. Also present in megalosaurids and *Allosaurus*); deep oblique ligament groove on posterior surface of femoral groove (ch.678; shared with most of theropods, but absent in *Afrovenator, Megalosaurus* and *Torvosaurus tanneri*); femoral head strictly medially directed in the anteroposterior plane (ch. 680; potential synapomorphy of Spinosauridae within megalosauroids, although also present in *Afrovenator*; outside megalosauroids, it is also present in allosauroids and Coelurosauria).

Synapomorphies in baryonychinae that also are present in *Riojavenatrix* are: posteromedially oriented long axis of medial condyle of femur in distal view (ch. 693; absent in *Spinosaurus* and other theropods, but unknown in *Ichthyovenator.* Also recovered in other taxa outside Spinosauridae); incomplete ossification in the fibular crest (ch. 710; present in *Suchomimus*, but unknown in *Baryonyx*; absent in other megalosauroids); bluntly rounded vertical ridge as buttress for astragalus in the tibia

(ch. 719; present in *Suchomimus* and *Riojavenatrix*, and distinct to the rest of megalosauroids and carnosaurs).

Synapomorphies in Spinosaurinae that also are present in *Riojavenatrix* are: Ascending process of astragalus offsets from astragalar body by a pronounced groove (ch. 739; present in *Spinosaurus* and *Riojavenatrix*, absent in *Suchomimus* and unknown in other spinosaurids; also present in *Wiehenvenator* within megalosauroids, and in some coelurosaurs).

Within Spinosauridae, baryonychines have following synapomorphies that are absent in *Riojavenatrix:* absence of an expanded pubic boot (Ch. 639; shared with *Afrovenator* within megalosauroids, some coelophysoids, some ceratosauria and alvarezsauroids); lateral malleolus projects far distal to medial malleolus (ch. 717; present in *Suchomimus*; but absent in *Spinosaurus* and *Riojavenatrix*, but is poorly coded in the matrix); anterior portion of fibular proximal end mediolaterally wider than the posterior portion (ch. 724; present in *Baryonyx* and other megalosauroids, but distinct to *Spinosaurus* and *Riojavenatrix*; some allosauroids and some Coelurosauria).

Within Spinosauridae, spinosaurines has following synapomorphies that are absent in *Riojavenatrix*: large and ovoid pubic obturator foramen (Ch. 652; shares with *Ichthyovenator* and *Spinosaurus*, also present in metricanthosaurids and *Concavenator*); low proximal projection of cnemial crest (ch. 702; present in *Spinosaurus*, but unknown in *Ichthyovenator* and *Baryonyx*; and absent in *Suchomimus*, other megalosauroids, allosauroids, coelophysoids and some ceratosaurs); low and rounded fibular crest (ch. 713; present in *Spinosaurus* and other theropods as *Asfaltovenator,* some ceratosaurs and coelurosaurs; but absent in *Suchomimus* and *Riojavenatrix* within spinosaurids); presence of deep oval fossa on medial surface of fibula (ch. 730; potential synapomorphy of spinosaurines within megalosauroids, but it is unknown in *Ichthyovenator,* also present in allosauroids); reduced and facing laterally fibular facet on astragalus (ch. 734; present in *Spinosaurus*, but absent in *Riojavenatrix* and other megalosauroids and carnosaurs, except *Mapusaurus*, but unknown in other spinosaurids).

The potential autapomorphy of *Riojavenatrix* within spinosaurids based on the phylogenetic analysis is: height of ascending process of the astragalus more than twice the height of astragalar body (ch. 735; present in *Riojavenatrix* but not in *Suchomimus* and other megalosauroids, also present outside spinosaurids, in *Allosaurus, Tyrannosaurus, Albertosaurus* and some derived coelurosaurs).

MATRIX MATEUS & ESTRAVIZ-LÓPEZ (2022)

The alternative phylogenetic analysis using the matrix proposed by Mateus & Estraviz-López (2022) resulted in 307 MPTs with a length of 1123 steps (CI:0.550; RI: 0.573). The strict consensus (Fig. 10A) shows a well-resolved topology in most of the monophyletic groups of theropods. Regarding results in non-spinosaurid groups, *Piatnitzkysaurus* is branched earlier in a polytomy of Carnosauria, and it is not recovered as a megalosauroid, unlike the results in Carrano *et al.* (2012). In Megalosauroidea, there is only a degree 5 polytomy formed by the megalosaurids *Afrovenator, Eustreptospondylus, Duriavenator* and *Dubreuillosaurus* (Afrovenatorinae in Carrano *et al.*, 2012) and the dichotomy of Megalosaurinae. Megalosaurinae (*Torvosaurus+Megalosaurus*) is a monophyletic group in these results. Within Spinosauridae, barynonychines (*Baryonyx+Suchomimus*) were recovered in a dichotomy. The rest of spinosaurids (including the new taxon *Riojavenatrix*) forms a degree 7 polytomy within the group, where the node of baryonychinae is also included.

Only three taxa are pruned from the iterPCR of this consensus as unstable and collapsing nodes in the strict consensus: *Eocarcharia, Monolophosaurus and Afrovenator*.. Other taxa are considered equally unstable, always forming polytomies even if they are pruned. These equally unstable taxa are: *Baryonyx, Iberospinus, Ichthyovenator, Irritator, Riojavenatrix, Spinosaurus, Suchomimus* and *Vallibonavenatrix*. Most of these taxa have scored characters that support alternative positions in different trees, so these characters should be re-evaluated to analyse the instability of these taxa. In addition, most spinosaurids show numerous missing data in their codings that if were scored, they

may help to resolve its position (Pol & Escapa, 2009). The IterPCR script analyses the missing data of each unstable taxon and evaluates their ancestral condition. If the missing characters have different optimization in the ancestral node of the problematic taxon in different MPTs, it implies that their scorings (if this is possible) may help to solve the instability of the taxon (Pol & Escapa, 2009). This is the case of *Riojavenatrix,* where if up to 113 of all missing data were scored, they may help to resolve its position (see Supplementary Material 2 for the list of these characters obtained in the IterPCR script results). However, all these characters are associated to missing bones or missing anatomical elements in the material of *Riojavenatrix*. If new material of this taxa is known in the future, all these characters should be re-evaluated and scored in following phylogenetic approaches, to define a stable position of *Riojavenatrix*. The agreement subtree (Fig. 10B) shows a dichotomy between *Suchomimus* and *Baryonyx*, which is the only dichotomy that is consistent in all the MPTs, and they are the only taxa that have been not considered as unstable and pruned. All the other spinosaurids are equally considered as unstable and there are six possible combinations of agreement subtrees (see list of pruned taxa in Supplementary Material 2). This result is partially consistent with the IterPCR one, but the later one considers all the spinosaurids as equally unstable (including *Suchomimus* and *Baryonyx*). Following the methodology for pruning trees incorporated in TNT (*prunnelsen*), the node 31 was improved if *Afrovenator* is pruned, the node 30 is improved if *Monolophosaurus* is pruned and, finally, the node 29 is improved if *Eocarcharia* is pruned. The results from IterPCR and *prunnelsen* are similar as for the taxa unstable and pruned (*Afrovenator, Monolophosaurus and Eocarcharia*), since both methodologies have similar stopping rules (Pol & Escapa, 2009). However, the equally unstable taxa in its politomy (spinosaurids) are not taken into consideretaion in the Pruned methodology of TNT, but they are in the IterPCR. Regarding the agreement subtrees, its algorithm continues pruning taxa until the subtree is dichotomous, and for that, this method does not prune the same most unstable taxa, as the other above mentioned, and keeps *Suchomimus* and *Baryonyx* as stable taxa because they form a dichotomy in all the subsets. Therefore,

although *Iberospinus* and *Riojavenatrix* are left in the agreement subtree, they should still be considered as unstable taxa as was inferred from the iterPCR.

The Bremer support analysis (all taxa included) shows many clades with minimal support. This is the case of Spinosauridae that show a Bremer support of 2. Jackknife and Bootstrap analyses have values below 50% in some groups, especially within Megalosauroidea. Spinosaurids are supported by 35 (Jackknife) and 14 (Bootstrap) (Fig. 10A).

The unambiguous synapomorphies (see Supplementary Material 2) from the strict consensus for spinosaurids are: presence of webbing at base of neural spines in dorsal vertebrae (ch. 179); accessory centrodiapophyseal lamina in dorsal vertebrae (ch. 180); expanded infraprezygapophyseal fossa in dorsal vertebrae (ch. 181). However, these characters are missing data in *Riojavenatrix*. The ambiguous synapomorphies that are shared by *Riojavenatrix* and others spinosaurids are (see SI for the complete list): large and oval obturator foramen of pubis (ch. 285; present in *Ichthyovenator* and *Riojavenatrix*); expanded and triangular morphology of distal end of ischium (ch. 297; present in *Ichthyovenator*, *Riojavenatrix and Vallibonavenatrix*; but absent in *Baryonyx* or *Suchomimus*); posteromedial orientation of medial condyle of femur in distal view (ch. 312; present in *Baryonyx, Riojavenatrix* and *Suchomimus*); bluntly rounded vertical ridge on medial side as buttress for astragalar in the tibia (ch. 320, present in *Riojavenatrix* and *Suchomimus*); fibular flange is not extended to proximal end of the tibia (ch. 322; present in *Riojavenatrix* and *Suchomimus)*; and almost double height of the ascending process respect to the height of astragalar body (ch. 331; present in (ch. State 2): *Riojavenatrix* and *Suchomimus*).

COMPARISONS WITH SPINOSAURIDAE AND OTHER THEROPODS

Results from phylogenetic analysis support a placement of *Riojavenatrix* within the Spinosauridae. This new taxon has a unique combination of spinosaurid characters supporting this placement, according to the phylogenetic analysis performed with the matrix of Rauhut & Pol (2021): (1) a pubic

apron that extends from the middle of the pubic shaft, (2) a deep oblique ligament groove on posterior surface of femoral groove, and (3) femoral head strictly medially directed in the anteroposterior plane.

Within Spinosauridae, *Riojavenatrix* shares three synapomorphies with members of Baryonychinae in the first phylogenetic analysis: (1) the postermedially oriented long axis of the medial condyle femur in distal view, (2) the incomplete ossification in the fibular crest, and (3) the bluntly rounded vertical ridge as buttress for astragalus in the tibia. However, *Riojavenatrix* shares only one synapomorphy with members of Spinosaurinae: the ascending process of astragalus offsets from astragalar body by a pronounced groove.

Its placement within Spinosauridae is supported by six ambiguous synapomorphies according to the results from the phylogenetic analysis performed with the Mateus & Estraviz-López (2022) matrix: (1) a large and oval pubic obturator foramen, (2) expanded and triangular morphology of distal end of ischium, (3) the posteromedially oriented long axis of the medial condyle femur in distal view (Baryonychinae synapomorphy based on the first phylogenetic analysis using Rauhut & Pol, 2021 matrix); (4) the bluntly rounded vertical ridge as buttress for astragalus in the tibia (Baryonychinae synapomorphy based on the first phylogenetic analysis using Rauhut & Pol, 2021 matrix); (5) fibular flange is not extended to proximal end of the tibia due to incomplete ossification (Baryonychinae synapomorphy based on the first phylogenetical analysis using Rauhut & Pol, 2021 matrix); (6) the height of the ascending process of the astragalus doubling the height of the astragalar body. Therefore, this unique combination of spinosaurid synapomorphies based on two phylogenetic analysis implies that *Riojavenatrix* can confidently be regarded as a spinosaurid.

The fossil record of Spinosauridae is in most cases fragmentary, with only a few well-known taxa. Comparison between the spinosaurid fossil record is limited by the absence of overlapping material between *Riojavenatrix* and the European *Ceratosuchops* and *Riparovenator*, the African *Cristatusaurus* and *Sigilmassasaurus*, and the South American *Angaturama*, *Irritator* Martill *et al.*, 1996 and *Oxalaia*. Nevertheless, the fossil remains of *Riojavenatrix lacustris* overlap with enough

material of other African, Asian and European spinosaurids (Charig & Milner, 1997; Sereno *et al.*, 1998; Allain *et al.*, 2012; Ibrahim *et al.*, 2014; Sánchez-Hernández & Benton, 2014; Malafaia *et al.*, 2018, 2020a; Mateus & Estraviz-López, 2022) allowing to make comparisons and evaluate the possible synonymy between them, especially between the herein described taxon and the other Iberian spinosaurids.

PELVIC GIRDLE

Pubis: Riojavenatrix preserves an obturator notch in the pubis like several tetanurans and more derived theropods (Hutchinson, 2001). The preserved diaphysis of the pubis in *Riojavenatrix* is straight and similar to that of *Baryonyx* (NHMUK VP R9951), *Iberospinus* (Mateus & Estraviz-López, 2022), *Ichthyovenator* (MDS-Savannakhet BK10-11) and *Suchomimus* (MNN GDF500), and unlike the curved shaft of FSAC-KK 11888. In *Iberospinus*, a longitudinal groove extends along the pubic shaft, a feature that is also present, but subtly, in *Ichthyovenator* (Mateus & Estraviz-López, 2022) and also *Baryonyx* (NHMUK VP R9951). This groove is not present in the preserved shaft of *Riojavenatrix*, since it is present on the proximal end of the pubic shaft. The pubic apron of *Riojavenatrix* would have reached or almost the pubic boot and extends much further distally than in *Baryonyx* (NHMUK VP R9951), *Ichthyovenator* (MDS-Savannakhet BK10-11) and *Suchomimus* (MNN GDF500). The distal position of the pubis apron of *Riojavenatrix* also differs from that of FSAC-KK 11888, because, in the latter, it does not reach the pubic boot. In distal view, the triangular-shaped distal end of the pubis of *Riojavenatrix* resembles that of *Ichthyovenator* (MDS-Savannakhet BK10-11) and megalosaurids (Fig. 11A–B). However, in *Ichthyovenator* (MDS-Savannakhet BK10-11) the lateral surface is much more concave (Fig. 11B), giving it an L-shaped distal outline (Allain *et al.*, 2012) as compared to the more triangular pubic boot of *Riojavenatrix* in distal view (Fig. 11A). This triangular-shaped pubis in distal end is related to a strong mediolateral expansion of the anterior part of the pubic boot, which was proposed as a Baryonychinae feature (Sereno *et al.*, 1998; Allain *et al.*, 2012). However, the pubic boots of FSAC-KK 11888, *Baryonyx* (NHMUK VP R9951) and *Suchomimus* (MNN GDF500) are much narrower mediolaterally through their whole anteroposterior

length in distal view than those of *Ichthyovenator* (MDS-Savannakhet BK10-11) and *Riojavenatrix* (Fig. 11A–E). In *Suchomimus* (MNN GDF500) and *Baryonyx* (NHMUK VP R9951), a subtle L-shape can be noticed in distal view whereas it is more oval in FSAC-KK 11888, differing from *Riojavenatrix* (Fig. 11A, C–E).

Ischium: The iliac peduncle of the ischium of *Riojavenatrix* shows a planoconcave articulation, a feature shared with *Baryonyx* (NHMUK VP R9951), FSAC-KK 11888 and *Suchomimus* (MNN GDF500). According to Allain *et al.* (2012) and Malafaia *et al.* (2020a), the articulation of the ischium with the ilium is peg-and-socket in *Ichthyovenator* and *Vallibonavenatrix*. Nevertheless, the morphology of these iliac peduncles in the latter taxa have a similar morphology to other spinosaurids (i.e., planoconcave); and they do not have the well-developed and deep excavated fossa on the iliac peduncle, referred as this peg-and-socket articulation, featured in abelisauroids and carcharodontosaurians (Sereno *et al.*, 2004; Carrano *et al.*, 2012). Therefore, all spinosaurids have a planoconcave articulation of the ischium for the ilium, a feature also seen in *Riojavenatrix*. In proximal view, the iliac articulation is less anteroposteriorly elongate in *Riojavenatrix* than in *Baryonyx* (NHMUK VP R9951) and FSAC-KK 11888, resembling that of *Ichthyovenator* (MDS-Savannakhet BK10-12–13), *Suchomimus* (MNN GDF500) and *Vallibonavenatrix* (MSMCa-1–3). The latter two also have a medially positioned and anteroposteriorly oriented crest with an adjacent groove on the medial surface of the acetabulum (Malafaia *et al.*, 2020a). In *Baryonyx* (NHMUK VP R9951), a similar anteroposteriorly oriented groove is present. This is also lateral and medially bounded by two low, rounded and parallel ridges that, together with the groove, fade anteriorly. Despite *Riojavenatrix* having a similar crest, it lacks the adjacent groove. In lateral view, the preserved portion of the ischial diaphysis and the distal portion of the *Riojavenatrix* ischium are more slender than those of FSAC-KK 11888, *Ichthyovenator* (MDS-Savannakhet BK10-12–13), *Suchomimus* (MNN GDF500) and *Vallibonavenatrix* (MSMCa-1–3). The anterior margin of the shaft and the distal portion of the *Riojavenatrix* ischium are transversely proportionately as thick as in *Suchomimus* (MNN GDF500) and *Vallibonavenatrix* (MSMCa-1–3). Nevertheless, the ischial boot

expands further anteroposteriorly in respect to the shaft in *Riojavenatrix* than in FSAC-KK 11888, *Ichthyovenator* (MDS-Savannakhet BK10-12–13), *Suchomimus* (MNN GDF500) and *Vallibonavenatrix* (MSMCa-1–3) (Fig. 11F–J). In FSAC-KK 11888, the distal expansion is posteriorly directed, further differing from the *Riojavenatrix* ischium. The ischial boot is rounded in lateral view in FSAC-KK 11888 and *Suchomimus* (MNN GDF500), whereas it is more triangular in *Ichthyovenator* (MDS-Savannakhet BK10-12–13), *Vallibonavenatrix* (MSMCa-1–3) and *Riojavenatrix* (Fig. 11F–J). Nevertheless, the anterodistal surface of the ischial boot is only angular in *Riojavenatrix*. Furthermore, the anterior tip of the ischial boot in *Riojavenatrix* resembles that of *Megalosaurus* Buckland, 1824 (OUMNH J.13565; Benson, 2010, fig. 15G–L). This tip is not as marked in *Ichthyovenator* (MDS-Savannakhet BK10-12–13), and it is not present in FSAC-KK 11888, and not preserved in *Suchomimus* (MNN GDF500) and *Vallibonavenatrix* (MSMCa-1–3) (Fig. 11F–J).

HINDLIMB

Femur: The femora of *Riojavenatrix* shows several similarities with megalosauroid theropods (Fig. 12), such as the rounded medial epicondyle and the small rugose patch for the attachment of the *M. femorotibialis externus* (Carrano *et al.*, 2012). Furthermore, like other spinosaurids, the medial condyle of the left femur of *Riojavenatrix* has a posteromedial orientation (Benson, 2010) and not posterolateral as previously suggested by some authors (e.g., Benson, 2010; Carrano *et al.*, 2012; Malafaia et al., 2018). Nevertheless, the posteromedial displacement in the new taxon is remarkably much less marked than in *Baryonyx* (NHMUK VP R9951), FSAC-KK 11888, "*Spinosaurus* B" (Nr. 1922 X 45; Stromer, 1934) and *Suchomimus* (MNN GDF500) and more similar to CMP-3b/211 (Fig. 12A-F). Indeed, this condition is somewhere between that of these spinosaurids and other megalosauroids like *Megalosaurus* (NHMUK PV 31806; Benson 2010, fig. 16I–J). The distal end of the *Riojavenatrix* femur also differs from *Baryonyx* (NHMUK VP R9951) and FSAC-KK 11888 in the distal extension of the lateral condyle. This distal end projects further distally than the medial condyle in *Baryonyx* (Charig & Milner, 1997; Carrano *et al.*, 2012) and the right femur of FSAC-KK

11888. In *Riojavenatrix* instead, the femoral condyles are almost equally projected, a feature also seen in CMP-3b/211, "*Spinosaurus* B" (Nr. 1922 X 45) and *Suchomimus* (MNN GDF500). Furthermore, the femoral condyles in FSAC-KK 11888 are notably narrower (Fig. 12A, F) and its fourth trochanter is hypertrophied (Ibrahim *et al.*, 2014). The main axis of the lateral condyle of *Baryonyx* (NHMUK VP R9951) and FSAC-KK 11888 is more anteroposteriorly directed and also narrower than in *Riojavenatrix* (Fig. 12A, D, F). In *Riojavenatrix*, the lateral condyle is almost as rounded and broad as that of *Suchomimus* (MNN GDF500) with a similar orientation, and virtually identical to CMP-3b/211 (Fig. 12A, B, E). The extensor groove is also more developed in *Baryonyx* (NHMUK VP R9951), "*Spinosaurus* B" (Nr. 1922 X 45) and FSAC-KK 11888 than in *Riojavenatrix,* and this is more similar to that of *Suchomimus* (MNN GDF500) and CMP-3b/211 (Fig. 12A–F). The flexor groove in *Baryonyx* is also wider and deeper compared to *Riojavenatrix* (NHMUK VP R9951). The head of the femur of *Riojavenatrix* is quite subcircular as in CMP-MS-0/22, CMP-3b/211, *Baryonyx* (NHMUK VP R9951) and *Suchomimus* (MNN GDF500), and it differs from that of FSAC-KK 11888, which is more oval in medial view. The articular groove of the proximal surface of the right femur resembles that of CMP-MS-0/22 and CMP-3b/211, due to the latter ones being relatively narrow and deep (Malafaia *et al.*, 2018) (Fig. 12G–J). However, in *Baryonyx* (NHMUK VP R9951) and *Suchomimus* (MNN GDF500), the proximal articular grooves are relatively broader and not as restricted, at least, posterolaterally (Fig. 12I–J). Furthermore, this articular groove is more anteriorly located and anteroposteriorly oriented in *Riojavenatrix* (Fig. 12G). *Riojavenatrix* also lacks the longitudinal V-shaped groove present on the medial surface of the shaft of *Baryonyx* (Charig & Milner, 1997). In the FSAC-KK 11888 femora, the crista tibiofibularis is more posteriorly projected in distal view than in *Riojavenatrix* (Fig. 12F). The CMP-MS-0/22 and CMP-3b/211 femora almost exclusively differ from those of *Riojavenatrix* in the bowing of the femoral shaft, being CMP-3b/211 straighter in lateral view, and with a slightly broader tibiofibular crest.

Tibia: The supraastragalar buttress of *Riojavenatrix* is a vertical ridge located on the medial side, a feature also shared with *Chilantaisaurus* Hu, 1964 (Benson & Xing, 2008), CMP-3c/188, FSAC-KK

11888 and *Suchomimus* (Rauhut, 2003; Benson & Xing, 2008; Carrano *et al.*, 2012; Malafaia *et al.*, 2018). The shaft of the left tibia of *Riojavenatrix* is straight, whereas in CMP-3c/188 it is medially curved distally due to the medially projected medial malleolus (Malafaia *et al.*, 2018). In *Suchomimus* (MNN GDF500), the tibial shaft is laterally bowed, a feature also observed, but to a lesser extent, in FSAC-KK 11888. Unlike in *Riojavenatrix*, the shaft of the *Camarillasaurus* tibia is "G-shaped" due to a deep groove present posteriorly on its lateral surface (Sánchez-Hernández & Benton, 2014). This structure is also described in the left tibia of FSAC-KK 11888 (Samathi *et al.*, 2021). However, this could be the result of preservation or pathology (Samathi *et al.*, 2021). *Riojavenatrix* further differs from CMP-3c/188 in lacking the concavity situated posterior to the fibular crest that bears a tibial foramen (Malafaia *et al.*, 2018). *Suchomimus* (MNN GDF500) has a proximodistally oriented groove that is parallel and anterior to the fibular flange. In *Camarillasaurus*, this is a subtle depression and has a distally located foramen (Sánchez-Hernández & Benton, 2014). These are not present in *Riojavenatrix*. The cnemial crest follows the same pattern of *Camarillasaurus*, FSAC-KK 11888 and *Suchomimus*, where the tibia narrows towards the anteriormost part of this structure (Samathi *et al.*, 2021). However, in *Riojavenatrix*, the tip of the cnemial crest is more laterally directed, differing from that of *Camarillasaurus* (MPG-KPC8), FSAC-KK 11888, "*Spinosaurus* B" (Nr. 1922 X 45) and *Suchomimus* (MNN GDF500) (Fig. 13A, C–E), and being more similar to other non-spinosarid theropods such as *Allosaurus* Marsh, 1877 (USNM 4734, Gilmore, 1920, fig. 49), *Condorraptor* Rauhut, 2005, *Fukuiraptor* Azuma & Currie, 2000 (FPMN 9712220; Azuma & Currie, 2000, fig. 13C), *Megalosaurus* (NHMUK PV 31809; Benson, 2010, fig. 17G), *Sinraptor* Currie & Zhao, 1993 (IVPP 10600; Currie & Zhao, 1993, fig. 22I) and *Tyrannosaurus* Osborn, 1905 (Brochu, 2003). In addition, the cleft between both tibial condyles is narrower in *Riojavenatrix* than in *Camarillasaurus* (MPG-KPC8) ('intercondylar groove' of Sánchez-Hernández & Benton, 2014), "*Spinosaurus* B" (Nr. 1922 X 45) and FSAC-KK 11888, and it is more similar to that present, for instance, in *Suchomimus* (MNN GDF500) and *Megalosaurus* (Benson, 2010) (Fig. 13B–E). Furthermore, in *Riojavenatrix* the

lateral process of the lateral condyle of the tibiae are proximodistally longer and narrower than the shorter and triangular one of *Camarillasaurus* (MPG-KPC8).

Distally, the supraastragalar buttress is more marked and thinner in *Riojavenatrix* than in CMP-3c/188. This crest smoothly inclines laterally in CMP-3c/188 and rises from the medial edge of the tibia, whereas it is more angular and with its distalmost end being located on the anterior side of the tibia in *Riojavenatrix*. This feature is similar in *Suchomimus* (MNN GDF500), but the tibia is slightly damaged at this point. The distal portion of the supraastragalar buttress is more inclined in FSAC-KK 11888 than in *Riojavenatrix*. The facet for the ascending process of the astragalus of the *Riojavenatrix* tibia is not as broad as in CMP-3c/188 and *Suchomimus* (MNN GDF500), occupying slightly more than half of the anterior surface of the tibia distally, but it extends almost as high as in the latter taxa. The mediolateral extension of this facet in *Riojavenatrix* is certainly more similar to FSAC-KK 11888, but in the latter the apicalmost point of the facet is more centrally placed. On the posterior side, the CMP-3c/188 tibia shows a marked concavity between the lateral malleolus and a vertical triangular crest (Malafaia *et al.*, 2018), which is a slight depression in *Riojavenatrix*. The angle between the tibial malleoli is also much higher in CMP-3c/188 than in *Riojavenatrix*, being in the latter one more angular, straighter and almost equally directed distally. In this feature, the tibia of *Riojavenatrix* resembles the specimen of FSAC-KK 11888 and somewhat that of *Suchomimus* (MNN GDF500). However, the lateral malleoli of FSAC-KK 11888 and *Suchomimus* (MNN GDF500) are slightly more distally projected than in *Riojavenatrix*. In posterior view, the distal margin between the tibial malleoli of *Riojavenatrix* is straight, like in *Suchomimus* (MNN GDF500). In FSAC-KK 11888, there is a concavity like in CMP-3c/188 (Malafaia *et al.*, 2018), which is more pronounced in the latter specimen. The distal expansion of the *Riojavenatrix* tibia is not as pronounced as in *Suchomimus*, because the lateral malleolus is larger and projects further laterally in *Suchomimus* (MNN GDF500) than in *Riojavenatrix*. This projection in *Riojavenatrix* resembles that of CMP-3c/188 and FSAC-KK 11888.

Fibula: Compared to other spinosaurids, the fibula of *Riojavenatrix* is more slender. As in other megalosauroid theropods, the fibula of *Riojavenatrix* shows a shallow medial fossa (*sensu* Carrano *et al.*, 2012) or lacks the medial depression (*sensu* Benson, 2010 and Rauhut *et al.*, 2016), differentiating them from most of other neotheropods. In proximal view, the *Riojavenatrix* fibula shows a comma-shaped outline. However, this is posteriorly straighter than in *Wiehevenator* Rauhut *et al.*, 2016 (WMN P27479 and 27502) and it thinners posteriorly more than in *Baryonyx* (NHMUK VP R9951; note that the better preserved *Baryonyx* fibula is here regarded as a left one), *Camarillasaurus* (MPG-KPC unnumbered) and FSAC-KK 11888. Moreover, the fibula is more C-shaped in proximal view in *Baryonyx* (NHMUK VP R9951; crescent-shape of Charig & Milner, 1997) and FSAC-KK 11888. In medial view, the posterior margin of the proximal end in *Baryonyx* is more proximally projected than the anterior edge in *Riojavenatrix*. In *Baryonyx* (NHMUK VP R9951), it is also more elevated but less pronounced, and distinguishes from *Camarillasaurus* (MPG-KPC unnumbered) and FSAC-KK 11888, which have an almost even proximal end. The medial fossa is deeper in FSAC-KK 11888 and proportionally shallower in *Baryonyx* (NHMUK VP R9951) compared to *Riojavenatrix*. Instead, *Riojavenatrix* has a medial fossa on the fibula that resembles that of *Suchomimus* (MNN GDF500). Nevertheless, the distal end of the fossa is more acute in *Riojavenatrix* than in *Suchomimus* (MNN GDF500), but more rounded than that of *Baryonyx* (NHMUK VP R9951) and FSAC-KK 11888. This fossa extends more distally in *Baryonyx* (NHMUK VP R9951) and FSAC-KK 11888 than in *Riojavenatrix*, which is similar to *Suchomimus* (MNN GDF500). The proximal expansion of the fibula is more abrupt in *Riojavenatrix* than in FSAC-KK 11888, especially the posterior blade. This blade is blunter in *Riojavenatrix* than in *Baryonyx* (NHMUK VP R9951). Below the medial fossa, the iliofibularis tubercle is not especially marked in *Riojavenatrix* and so similar to the condition observed in FSAC-KK 11888 and *Suchomimus* (MNN GDF500). In *Baryonyx* (NHMUK VP R9951), this is even less noticeable and lacks the groove present in the herein described taxon.

Astragalus: The distal condyles of the astragalus are anterodistally projected in *Riojavenatrix* with an angle similar to other tetanurans (Sereno *et al.*, 1996; Carrano *et al.*, 2012). In addition to the herein

described one, solely another, and yet undescribed, spinosaurid astragalus is known (MNN GDF unnumbered and referred to *Suchomimus* according to Rauhut, 2003). The ascending process of the latter astragalus is taller than that of *Allosaurus* (Sereno *et al.*, 1998). In *Suchomimus*, the ascending process of the astragalus is higher than the astragalar body, a feature also proposed for Spinosauridae among early-branching tetanurans (Carrano *et al.*, 2012). Indeed, the ascending process for this astragalus is 1.6 times taller than its body in that referred to *Suchomimus* (Carrano *et al.*, 2012). The ascending process of the astragalus of *Riojavenatrix* is taller than its body like the one referred to *Suchomimus*. Nevertheless, this is even taller in *Riojavenatrix,* doubling the height of the astragalar body. Due to the absence of other spinosaurid astragali, it is difficult to compare the *Riojavenatrix* astragalus with other taxa. Therefore, it is not possible to assess if the vertical ridge on the medial margin of the ascending process of the astragalus is an autapomophy of *Riojavenatrix* or a synapomorphy among Spinosauridae.

Calcaneum. The *Riojavenatrix* calcaneum is smaller in size than those of *Baryonyx* (NHMUK VP R9951) and *Iberospinus* (ML1190-31) (Fig. 14). This calcaneum is especially mediolaterally narrower and higher than that of *Iberospinus* (ML1190-31) (Fig. 14A–B). Moreover, the calcaneum of *Riojavenatrix* bears a foramen located in an anterolateral depression which is so far only present in this taxon. The calcaneum of *Baryonyx* (NHMUK VP R9951) differs from the one of *Riojavenatrix* in having a centrally located large depression and several, but smaller, foramina and from *Iberospinus* (ML1190-31) because the latter lacks any of them (Fig. 14A–C). Furthermore, the astragalar facet of *Baryonyx* bears two fossae (Charig & Milner, 1997) that are not present in *Riojavenatrix*.

Pes: Pedal elements are scarce and usually fragmentary among Spinosauridae. The hourglass-shaped proximal end of the third metatarsal of *Riojavenatrix* is also present in other tetanurans (Carrano *et al.*, 2012). This metatarsal is robust in *Riojavenatrix* resembling the shape of those of *Chilantaisaurus* (Benson & Xing, 2008), *Sinraptor* (Currie & Zhao, 1993) and *Torvosaurus* Galton & Jensen, 1979 (Britt, 1991). In addition, unlike avetheropods, the cross-section of the shaft of the metatarsal III of *Riojavenatrix* is rectangular, similar to early-branched tetanuran theropods (Carrano *et al.*, 2012).

Charig & Milner (1997) mentioned the presence of two distal ends of metatarsal bones belonging to *Baryonyx*, indicating that they could belong to metatarsal II, III or IV. Despite these being quite fragmentary, they have been here identified as the distal ends of the metatarsals II and III. The metatarsal that is not ginglymoid would correspond to the distal end of metatarsal III and the other to the distal end of metatarsal II, due to the latter showing a ventral groove and being mediolaterally broad in distal view compared to the distal ends of metatarsals IV. Furthermore, the metatarsal assigned to the digit II, is too dorsoventrally low for it to be considered from digit IV. In distal view, the third metatarsal of *Riojavenatrix* is not ginglymoid, a condition also present in other megalosauroids like *Baryonyx* (NHMUK VP R9951), *Megalosaurus* (Benson, 2010) and other theropods (Norell *et al.*, 2001). In *Riojavenatrix,* the distal condyle is much mediolaterally broader than in the metatarsal III of *Baryonyx* (NHMUK VP R9951). Furthermore, this is square-shaped and dorsoventrally larger than mediolaterally wide in *Baryonyx* (NHMUK VP R9951). Moreover, the ventral margin of the distal condyle of the metatarsal III of *Riojavenatrix* is concave whereas it is flat in *Baryonyx* (NHMUK VP R9951).

Many spinosaurid pedal unguals from Gondwanan formations have been reported, and all of them show a flat ventral side (see Stromer, 1934; Novas *et al.*, 2005; Ibrahim *et al.*, 2014; Maganuco & Dal Sasso, 2018; de França *et al.*, 2021). Ibrahim *et al.* (2014) reconstructed the pes of FSAC-KK 11888 with also a flat-bottomed I-2. This is not the case for the I-2 phalanx of *Riojavenatrix* which is remarkably curved. Furthermore, the pedal unguals of FSAC-KK 11888 are broader than deep, differing from the preserved I-2 phalanx of *Riojavenatrix*. The pedal ungual phalanx of *Baryonyx* (NHMUK VP R9951) does not show a flat ventral side and bears a longitudinal groove on each side. The ventral surface of *Iberospinus* (Mateus & Estraviz-López, 2022) is flatter than that of other European spinosaurids, but its preservation does not permit a more precise comparison. A single longitudinal groove in pedal unguals is a plesiomorphy found among early-branched theropods, with the exception of Abelisauroidea, where two bifurcating grooves are present (Carrano & Sampson, 2008). The I-2 pedal ungual of *Riojavenatrix* only shows one longitudinal groove on the lateral side

whereas it is devoid of it on the medial side. Therefore, it differs from most other theropods in this feature (e.g., *Alectrosaurus* Gilmore, 1933 (Mader *et al.*, 1989); *Bambiraptor* Burnham *et al.*, 2000; *Deinonychus* Ostrom, 1969; *Tyrannosaurus* (Brochu, 2003): FMNH PR2081; and an indeterminate carcharodontosaurian from Portugal (Malafaia *et al.*, 2019)) (Fig. 15). But also, it differs from all the so far described spinosaurid ungual phalanges, which have a longitudinal groove on the medial side of the pedal ungual phalanges (see Stromer, 1934; Charig & Milner, 1997; Novas *et al.*, 2005; Ibrahim *et al.*, 2014; Maganuco & Dal Sasso, 2018; de França *et al.*, 2021; Mateus & Estraviz-López, 2022). Therefore, the presence of a longitudinal groove on the lateral surface of pedal phalanx I-2 and the absence of it on the medial side may be an autapomorphy of *Riojavenatrix*. Nevertheless, the absence ofpedal unguals that can be confidently attributed to digit I in other spinosaurids, or even in Megalosauroidea, prevents this assertion with certainty because it can also be a synapomorphy of any of the latter groups.

HISTOLOGICAL ANALYSIS

Bone sections show, in general, a 5 to 10 mm-thick moderately thin cortex of primary compact bone, which grades into a large medullary region completely filled by bony trabeculae (Fig. 16A–B). Bone microstructure is too poorly preserved for a precise histological assessment due to the intense diagenesis and low-grade metamorphism experienced by the sediments of the Enciso Group (see Geographical and geological setting). Therefore, the bone matrix microstructure and type of the primary vascularity are not recognizable. However, some general patterns of the bone microstructure can be identified in the recovered material. In this sence, clusters of Haversian systems are clearly identifiable in the innermost region of the compacta (Fig. 16E), where at least two overlapping generations of secondary osteons are visible. Isolated secondary osteons and large resorption rooms incompletely filled by lamellar bone (i.e., incipient secondary osteons) are also present on the peripheral regions of the compacta. When present, they tend to be organized in circular rows, in the same manner seen in other groups of dinosaurs (Company, 2011; Cerda *et al.*, 2017).

Other histological structures recorded in the cortex consist of well-defined lines of arrested growth (LAGs) which result in a cortical stratification. They are more evident in the external region of the compacta, where the secondary remodelling is less invasive (Fig. 16B–D). The presence of these growth lines indicates that the animal grew with a seasonal cyclicity, probably annual (D'Emic *et al.*, 2023 and references therein). As the subperiosteal surface of the bones has been partially eroded away by abrasion, it is not possible to determine if the external fundamental system, a proxy of somatic maturity composed of closely spaced resting lines, was once present in the samples.

The presence of large erosion spaces coated only by a thin layer of lamellar bone (i.e., immature Haversian osteons), and only two generations of secondary osteons with scarce overlapping, indicates that the processes of osteonal remodelling were not complete and were still active when the animal perished. This fact, along with the presence of intense secondary reconstruction in the internal perimedullary region, but scarce towards the outer cortex, combined with the existence of cyclical growth rings points to a somatically immature, still growing adult.

DISCUSSION

PHYLOGENETIC DISCUSSION AND IMPLICATIONS IN SPINOSAURIDAE

Spinosauridae, as a family, gathers members that are quite fragmentary, aside from them lacking plenty of overlapping material. However, some taxa are well represented, such as *Baryonyx*, *Irritator*, *Suchomimus* and FSAC-KK 11888. This fragmentary nature of the spinosaurid record is one of the main causes of the instability of this clade in the phylogenetical analyses. Most of the representative taxa of Spinosauridae are considered unstable in the parsimonious analyses of the two studied matrices. Three of these unstable taxa are Iberian representatives (*Camarillasaurus, Riojavenatrix,* and *Vallibonavenatrix*) based on the matrix of Rauhut & Pol (2021); and *Riojavenatrix, Iberospinus* and *Vallibonavenatrix* in the case of the Mateus & Estraviz-López (2022) matrix. This scarce record

leads to a lot of missing entries in these matrices. Some of these characters may help to determine the phylogenetic position of the unstable taxa if the scoring was established. In the case of *Riojavenatrix,* there are 113 characters (of a total of 534) that may help to resolve its position if they were scored based on the iterPCR method in the matrix of Mateus & Estraviz-López (2022). The scoring of these characters is not, hitherto, possible for *Riojavenatrix* because the elements are missing, but the analysis of which character could be supporting this instability allow to evaluate how the instability of this taxon is and the hypothetical reason of it, in order to improve it in future approach, re-evaluating all the problematic characters. However, the only record of this new taxon is mainly bones from the pelvic girdle and the hindlimb up to date, but a new individual is currently under study, which was recovered in a closeby locality. Despite the *Riojavenatrix* holotype not being a very complete skeleton, the recovered elements of it significantly overlap with other members of Spinosauridae, most importantly with all of those described in the Iberian Peninsula. Therefore, this allows us to compare in-depth this specimen with other members of Spinosauridae and, also, justify the establishment of a new taxon.

Although some of the features present in *Riojavenatrix* typically show up in Spinosauridae, some aspects are worth commenting. Spinosaurids show the "broadly triangular" outline of the pubic boot in distal view (Carrano *et al.*, 2012; char. 290). However, among spinosaurids this shape varies considerably. In *Baryonyx*, *Suchomimus* and FSAC-KK 11888, the pubes are quite lateromedially compressed and show a somewhat L-shape (*sensu* Allain *et al.*, 2012). *Ichthyovenator* still shows the L-shaped pubic boot (Allain *et al.*, 2012), but it is more triangular. If compared with these taxa, the *Riojavenatrix* pubic boot is virtually triangular in outline and quite robust. These features are similar to those characters found in the megalosaurids *Afrovenator* Sereno *et al.*, 1994 (MNBH TIG 1), *Eustreptospondylus* Walker, 1964 (OUMNHJ.13558) and *Streptospondylus* Meyer, 1832 (MNHN 8605).

The orientation of the medial condyle of the *Riojavenatrix* holotype femur is also unusual. This is posteromedially oriented, which is considered to be a synapomorphy of Spinosauridae (Charig &

Milner, 1997; Benson, 2010; Carrano *et al.*, 2012). This synapomorphy (311:1) was also listed from the results here obtained from the phylogenetic analysis of Mateus & Estraviz-López (2022). Nevertheless, the extent of this shifting compared to other non-spinosaurid theropods is much more marked in *Baryonyx* (NHMUK VP R9951), *Suchomimus* (MNN GDF500), "*Spinosaurus* B" (Nr. 1922 X 45), and, at least, the right femur of FSAC-KK 11888, and has an intermediate position in *Riojavenatrix*. The other Iberian spinosaurid femur from the Arcillas de Morella Formation (CMP-3b/211) shows this same trait. As the slightly posteromedially oriented medial condyle is present in two femora each from a different individual, the possible palaeopathological aftereffect for this character can be ruled out. Furthermore, this intermediate stage in the *Riojavenatrix* femora, together with the more similar distal outline of its pubic boot to other megalosaurid megalosaurians, may point to the hypothesis that *Riojavenatrix* could be an earlier branching spinosaurid.

Riojavenatrix is younger than *Baryonyx*, *Camarillasaurus*, *Ceratosuchops*, *Iberospinus* and *Riparovenator*, and most likely *Vallibonavenatrix*, coeval with *Ichthyovenator*, and *Suchomimus* (note the age of *Ichthyovenator* and *Suchomimus* is not very accurate) and older than the more derived mid Cretaceous African and South American spinosaurids (Charig & Milner, 1997; Sereno *et al.*, 1998; Allain *et al.*, 2012; Sánchez-Hernández & Benton, 2014; Sales & Schultz, 2017; Malafaia *et al.*, 2020a; Barker *et al.*, 2021; Mateus & Estraviz-López, 2022). Therefore, in the European basins there are seemingly more derived baryonychine spinosaurids (i.e., *Baryonyx*, *Ceratosuchops* and *Riparovenator*), with the latter two being closely related to *Suchomimus* (Barker *et al.*, 2021), and *Suchomimus* is a baryonychine that already shows both of the more derived features (i.e., a much mediolaterally narrow pubic boot and a more posteromedially oriented medial condyle of the femur). If additional skeletal remains of more complete specimens support this hypothesis, this spinosaurid would be one of the youngest baryonychines described hitherto and still remaining some plesiomorphic features.

SPINOSAURID PALAEOBIODIVERSITY IN THE IBERIAN PENINSULA

The Iberian Peninsula has yielded many spinosaurid remains that can shed light not only on the Iberian spinosaurid palaeobiodiversity, but also on the composition of Western Europe theropod faunas. The oldest Iberian putative spinosaurid remains come from the upper Hauterivian–lower Barremian Pinilla de los Moros Formation (Fuentes-Vidarte *et al.*, 2001; Canudo & Ruiz-Omeñaca, 2003). They consist of fragmentary elements regarded as *Baryonyx* sp. from the El Juguete site (Fuentes-Vidarte *et al.*, 2001). Nevertheless, this specimen does not belong to the genus *Baryonyx* and, possibly, neither to Spinosauridae due to the combination of the presence of a ridge on the anterior surface of the shaft, instead of a groove, and the absence of a paired anterior processes. The described chevron (MDS-Salas de los Infantes JBS,1) lacks an anterior longitudinal groove, which is present in *Baryonyx*, *Camarillasaurus*, SM-KK14 (Charig & Milner, 1997; Samathi *et al.*, 2021) and FSAC-KK 11888. In MDS-Salas de los Infantes JBS,1, instead, the anterior surface is convex, with a ridge appearing distally similar to the chevrons assigned to *Vallibonavenatrix* (Malafaia *et al.*, 2020a). Furthermore, MDS-Salas de los Infantes JBS,1 bears anterior processes, a feature apparently not present in Spinosauridae (Carrano *et al.*, 2012). It has been reported that these processes are not present in the preserved haemal arches of *Baryonyx*, *Riparovenator*, *Suchomimus,* SM-KK14 (Charig & Milner, 1997; Barker *et al.*, 2021; Samathi *et al.*, 2021) and apparently in *Vallibonavenatrix*. In *Camarillasaurus* (MPG-KPC45, 60 and 63) most of the preserved chevrons lack the anterior process, but the left anterior process is present in MPG-KPC47. Likewise, some of the *Baryonyx* (NHMUK VP R9951) and FSAC KK 11888 (O.W.M.R pers. comm.) chevrons seem to show anterior processes, but they are not as developed as in the El Juguete theropod. An isolated tooth studied by Torcida *et al.* (1997) from the Tenada de Costalomo site (MDS-Salas de los Infantes CLST,2), which is contemporaneous to the El Juguete specimen, would be the oldest definitive Iberian spinosaurid skeletal remains described up to date, if the El Juguete specimen is not regarded as a spinosaurid.

In the lower Barremian deposits of the Iberian Peninsula, spinosaurid remains become rather common, specifically in the Lusitanian and Maestrazgo basins. These remains mainly comprise isolated spinosaurid teeth (e.g., Infante *et al.*, 2005; Ruiz-Omeñaca *et al.*, 2005; Ruiz-Omeñaca, 2006;

Buffetaut, 2007; Sánchez-Hernández *et al.*, 2007; Gasca *et al.*, 2008, 2011, 2018; Mateus *et al.*, 2011; Figuereido *et al.*, 2015; Alonso & Canudo, 2016; Alonso *et al.*, 2018), but also postcranial remains (e.g., Gasca *et al.*, 2018) from the Blesa, Camarillas, El Castellar, Mirambel and Papo Seco formations (see Isasmendi *et al.*, 2020 and Malafaia *et al.*, 2020b for further information). Late Barremian skeletal remains regarded as Spinosauridae are also abundant, represented by isolated teeth (e.g., Ruiz-Omeñaca *et al.*, 1998; Canudo *et al.*, 2004, 2008) and less commonly postcranial remains (Malafaia *et al.*, 2018) from the Arcillas de Morella and Artoles formations in the Maestrazgo Basin (see Isasmendi *et al.*, 2020 and Malafaia *et al.*, 2020b for further information). In the Cameros Basin, late Barremian spinosaurid remains have also been described in different formations, but these may also be early Aptian in age (see e.g., Pereda-Suberbiola *et al.*, 2003; Torcida Fernández-Baldor *et al.*, 2003; Alonso *et al.*, 2017). The Enciso Group has also been dated as latest Barremian–early Aptian (Suarez-Gonzalez *et al.*, 2013). However, as the baryonychine remains described by Isasmendi *et al.* (2020, 2023) were recovered in the middle part of the group, they are highly likely Aptian in age, being probably the youngest spinosaurid remains described in Iberia up to date.

Despite most of the remains being fragmentary, several specimens have allowed to erect five different Iberian spinosaurid genera, aside from *Baryonyx*. *Camarillasaurus cirugedae* was first regarded as a basal ceratosaur (Sánchez-Hernández & Benton, 2014), but later identified as a member of Spinosauridae (Rauhut *et al.*, 2019; Barker *et al.*, 2021; Samathi *et al.*, 2021). Its phylogenetic position within Spinosauridae is still unresolved, being a spinosaurine for Barker *et al.* (2021), or an early member of Spinosauridae (Samathi *et al.*, 2021). The results after the iterPCR of the matrix Rauhut & Pol (2021) locate *Camarillasaurus* as a member of Spinosaurinae, with two alternative positions in this clade: (1) as an early spinosaurine; (2) as most related to *Ichthyovenator* than to *Spinosaurus*. The results of the reduced consensus by manually pruning are not enough to evaluate the position within the clade, because the Spinosaurinae was not recovered. This specimen comes from the Fuente Arnar outcrop of the lower Barremian Camarillas Formation (Maestrazgo Basin) (Sánchez-Hernández & Benton, 2004). *Iberospinus natarioi* is another early Barremian Iberian

spinosaurid (Mateus & Estraviz-López, 2022). This specimen, recovered from the Papo Seco Formation (Lusitanian Basin), was first assigned to *Baryonyx walkeri*, but its unusual features were also highlighted by Mateus *et al.* (2011). However, in a later revision and with the study of more material a new taxon was erected (Mateus & Estraviz-López, 2022). These authors proposed *Iberospinus* is closely related to baryonychines rather than spinosaurines. This taxon is not included in the Rauhut & Pol (2021) matrix, but in the second analysis that uses the matrix of Mateus & Estraviz-López (2022), *Iberospinus* and *Riojavenatrix* are closely related in the agreement subtree, supporting that the Portuguese taxon is more likely a baryonychine than a spinosaurine. The third Iberian spinosaurid, *Vallibonavenatrix cani*, comes from the younger Arcillas de Morella Formation, which is late Barremian in age (Malafaia *et al*., 2020a). This genus was first positioned within Spinosaurinae (Malafaia *et al*., 2020a). This position is also supported by Mateus & Estraviz-López (2022). However, in the phylogenetic analysis performed by Barker *et al.* (2021), the genus is recovered as a baryonychine or as an early spinosaurid, sister taxon of the node of Baryonychinae and Spinosaurinae. In our results, based on Rauhut & Pol (2021), the reduced consensus by iterPCR recovers *Vallibonavenatrix* in three different alternative positions: (1) as an early member of Spinosaurinae; (2) as a spinosaurine more close related to *Ichthyovenator* than to *Spinosaurus* (both results similar to those of Malafaia *et al.*, 2020a); but also (3) as a megalosaurid forming a clade with *Dubreuillosaurus* and *Leshansaurus* (the related position to *Leshansaurus* is also observed in the reduced consensus by manually pruning). Also from the same formation, the taxon *Protathlitis cinctorrensis* was erected (Santos-Cubedo *et al.*, 2023) and was recovered as the earliest baryonychine in the phylogenetic analysis carried out by Santos-Cubedo *et al.* (2023). The last erected genus is the herein described one, *Riojavenatrix lacustris*. The holotype individual was recovered from the uppermost Barremian–lower Aptian Enciso Group. However, the stratigraphic position of the Virgen del Villar- 1 locality within the group suggests an early Aptian age for *Riojavenatrix*. This spinosaurid was previously regarded as *Baryonyx* (Viera & Torres, 2013), but the osteological differences allow to differ this specimen from the British taxon. Here, in the reduced consensus by

iterPCR, *Riojavenatrix* is recovered in three alternative positions: (1) as baryonychine more related to *Baryonyx* than to *Suchomimus*; (2) as a baryonychine more related to *Suchomimus* than to *Baryonyx*; and (3) as a spinosaurine more related to *Ichthyovenator* than to *Spinosaurus* (probably due to the morphology of the ischial boot that is shared with *Vallibonavenatrix* and *Ichthyovenator* and supports this alternative position). Despite the fragmentary nature of these genera compared to other well-known theropods, the existing overlapping material supports the presence of five different spinosaurid taxa in Iberia (see also Malafaia *et al.*, 2020a, 2020b; Mateus & Estraviz-López, 2022).

Furthermore, the current and better known spinosaurid record does not back up the presence of *Baryonyx* in Iberia. Even the isolated teeth show differences that prevents their attribution to the genus. The teeth from the Castrillo de la Reina and Pinilla de los Moros formations of the Western Cameros Basin (MDS-Salas de los Infantes C-15,30; C-15,32; CLST,2; TBMV,13) were assigned to cf. *Baryonyx* by Torcida *et al.*, 1997. These teeth have flutes on both lingual and labial surfaces, feature not present in most of the teeth of the holotype of *Baryonyx* (Charig & Milner, 1997; Hendrickx *et al.*, 2019). Indeed, only one tooth shows both fluted sides with a single flute on the labial surface (Hendrickx *et al.*, 2019). These features are present (i.e., the presence of both fluted lingual and labial surfaces) in the baryonychine isolated tooth from the Boca do Chapim site (CPGP.1.06.2.), which was previously attributed to *Baryonyx* sp. by Figuereido *et al.* (2015) and, at least, the tooth of a right dentary fragment (MG 29A; Buffetaut. 2007), all from the Papo Seco Formation. Furthermore, another baryonychine isolated tooth (MNHN/UL.I.F2.176) also from Boca do Chapim site at least has five flutes on the labial surface (Malafaia *et al.,* 2013, 2020b) also differing from the teeth of the *Baryonyx* holotype. In the light of these considerations, the specimens differ significantly from the *Baryonyx* teeth; hence, they can assuredly be identified as baryonychine teeth, but not from the genus *Baryonyx*. Gasca *et al.* (2018) also described an isolated manual ungual phalanx from the El Castellar Formation (CSC1-4), regarding it as aff. *Baryonyx* sp. and already suggested it would likely belong to a spinosaurid different from *Baryonyx*. As the Iberian and European spinosaurid framework is becoming more complex, we here consider that CSC1-4 may better be regarded as Spinosauridae

indet. Therefore, all the fossil material previously attributed to *Baryonyx* does not belong to this genus, but to indeterminate baryonychines or spinosaurids.

The presence of different spinosaurid taxa in a restricted area and time interval has also been reported, for instance, in south-eastern England, with *Ceratosuchops* and *Riparovenator* from the Barremian Wessex Formation, and the large-sized indeterminate spinosaurid from the overlying upper Barremian Vectis Formation of the Wessex sub-basin, and *Baryonyx* from the Barremian Upper Weald Clay Formation of the Weald sub-basin (Charig & Milner, 1986, 1997; Barker *et al.*, 2021, 2022). The same has been suggested in other Gondwanan localities, such as the Araripe Basin, which has yielded the holotype specimens of the spinosaurines *Angaturama limai* and *Irritator challengeri* (Kellner & Campos, 1996; Martill *et al.*, 1996; Sales & Schultz, 2017; but see e.g., Charig & Milner, 1997; Sereno *et al.*, 1998, 2022; Buffetaut & Oujada, 2002; Dal Sasso *et al.*, 2005 for the possible synonymy), and also in the Kem Kem beds (Evers *et al.*, 2015), the Baharyia Oasis (Stromer, 1934) and the Elrhaz Formation (Taquet & Russell, 1998).

In Iberia, different baryonychine tooth morphotypes have been distinguished depending on the extension of the mesial carina and/or the presence or absence of mesial denticles (e.g., Ruiz-Omeñaca *et al.*, 1996; Canudo & Ruiz-Omeñaca, 2003; Ruiz-Omeñaca, 2006; Gasca *et al.*, 2008; Isasmendi *et al.*, 2020). This could suggest the presence of different baryonychine taxa or could be due to pseudoheterodonty (Canudo & Ruiz-Omeñaca, 2003; Ruiz-Omeñaca, 2006; Isasmendi *et al.*, 2020). Regardless, the presence of baryonychines and spinosaurines in the Lower Cretaceous deposits is well documented via dental elements (e.g., Infante *et al.*, 2005; Sánchez-Hernández *et al.*, 2007; Alonso *et al.*, 2017, 2018), even in the same site, such as La Cantalera-1 (Barremian, lower Blesa sequence; Aurell *et al.*, 2018), where both isolated baryonychine and spinosaurine teeth have been described (Alonso & Canudo, 2016). This supports the presence of at least two coeval spinosaurid taxa in Iberia. Concerning the Iberian spinosaurid taxa, *Camarillasaurus* and *Iberospinus* come from lower Barremian deposits from different basins (Sánchez-Hernández & Benton, 2014; Mateus & Estraviz-López, 2022), whereas *Vallibonavenatrix* is late Barremian (Malafaia *et al.*, 2020a) and

Riojavenatrix early Aptian in age. The former genus has only been reported in the Maestrazgo Basin whereas *Riojavenatrix* is present in the Cameros Basin.

CONCLUSIONS

The description of a partial skeleton from the uppermost Barremian–lower Aptian deposits of the Enciso Group (DS7) of Igea (La Rioja, Spain), has led to erect a new spinosaurid theropod genus and species, *Riojavenatrix lacustris*, gen. et sp. nov. This is the first theropod erected from the Cameros Basin and provides new knowledge to the barely known spinosaurid palaeodiversity of the Iberian Peninsula. Despite a poor preservation of *Riojavenatrix* bones, as the finest histological structures have been obliterated by diagenetical alteration, certain poorly preserved growth marks and osteonal remodeling processes remain visible in the bone. This suggests a somatically immature, still growing subadult individual. The performed phylogenetic results propose that *Riojavenatrix* is tentatively positioned as a Baryonychinae, although an alternative position within Spinosaurinae is also recovered. Moreover, *Riojavenatrix* and most other spinosaurids are considered unstable taxa in the phylogenies. *Riojavenatrix* corresponds to a medium- to large-sized spinosaurid dinosaur that differs from the other members of the clade due to the combination of a lateromedially thick and triangular pubic boot in distal view; an anteroposteriorly expanded and angular ischial boot with an anterodorsally oriented tip; a narrow, restricted and relatively deep proximal articular groove of the femur, which is anteromedially-posterolaterally inclined; a slightly posteromedially oriented medial femoral condyle; a longitudinal ridge on the medial margin of the ascending process of the astragalus (potential autapomorphy, but it could also be a character of Spinosauridae); height of ascending process of the astragalus more than twice the height of astragalar body (potential autapomorphy, but it could also be a character of Spinosauridae); an anterior depression with a dorsally located foramen on the lateral surface of the calcaneum; and the absence of any longitudinal groove on the medial surface of phalanx I-2 (potential autapomorphy, but it could also be a character of Spinosauridae or

even Megalosauroidea). Furthermore, the *Riojavenatrix* pubis and femur show features not as derived as other members of Spinosauridae. Spinosaurids were common in the Barremian faunas of Iberia, with the oldest definitive spinosaurid material (i.e., isolated baryonychine teeth) coming from the upper Hauterivian–lower Barremian deposits of Western Cameros Basin, and the youngest (i.e., *Riojavenatrix lacustris*, gen. et. sp. nov.) from the uppermost Barremian–lower Aptian of Eastern Cameros Basin. Furthermore, after the revision of other Iberian fossils regarded up to date to the genus *Baryonyx*, the presence of this genus in Portugal and Spain has been dismissed. Therefore, only five spinosaurid genera are here considered to be present in the Iberian Peninsula: *Camarillasaurus*, *Iberospinus*, *Protathlitis*, *Riojavenatrix* and *Vallibonavenatrix*.

DATA ARCHIVING STATEMENTS

The measurements of the holotype of *Riojavenatrix lacustris* are gathered in Supplementary material 1 and the phylogenetic data are included in Supplementary material 2. The data matrices are available on Supplementary File 1 and 2.

SUPPORTING INFORMATION

Additional supporting information can be found in the online-version of the article at the publisher's website:

Supplementary Material 1. Measurements of the holotype of *Riojavenatrix lacustris*.

Supplementary Material 2. Data of the phylogenetic analyses performed in the article.

Supplementary File S1: Rauhut & Pol, 2021 matrix in a nexus file.

Supplementary File S2: Mateus & Estraviz-Lopez, 2022 matrix in a nexus file.

REFERENCES

Allain R, Xaisanavong T, Richir P, Khentavong B. 2012. The first definitive Asian spinosaurid (Dinosauria: Theropoda) from the Early Cretaceous of Laos. *Naturwissenschaften* **99**: 369–377.

Alonso A, Canudo JI. 2016. On the spinosaurid theropod teeth from the early Barremian (Early Cretaceous) Blesa Formation (Spain). *Historical Biology* **28**: 823–834.

Alonso A, Mas JR. 1993. Control tectónico e influencia del eustatismo en la sedimentación del Cretácico inferior de la Cuenca de Los Cameros. In: Salas R, Martín-Closas C., eds. Estratigrafía del Cretácico de la Península Ibérica I. *Cuadernos de Geología Ibérica* **17**: 285–310.

Alonso A, Canudo JI, Fernández-Baldor FT, Huerta P. 2017. Isolated theropod teeth associated with sauropod remains from El Oterillo II (Early Cretaceous) site of Salas de los Infantes (Burgos, Spain). *Journal of Iberian Geology* **43**: 193–215.

Alonso A, Gasca JM, Navarro-Lorbés P, Rubio C, Canudo JI. 2018. A new contribution to our knowledge of the large-bodied theropods from the Barremian of the Iberian Peninsula: the "Barranco del Hocino" site (Spain). *Journal of Iberian Geology* **44**: 7–23.

Arden TM, Klein CG, Zouhri S, Longrich NR. 2019. Aquatic adaptation in the skull of carnivorous dinosaurs (Theropoda: Spinosauridae) and the evolution of aquatic habits in spinosaurids. *Cretaceous Research* **93**: 275–284.

Aurell M, Soria AR, Bádenas B, Liesa CL, Canudo JI, Gasca JM, Moreno-Azanza M, Medrano-Aguado E, Meléndez A. 2018. Barremian synrift sedimentation in the Oliete sub-basin (Iberian Basin, Spain): Palaeogeographical evolution and distribution of vertebrate remains. *Journal of Iberian Geology* **44**: 285–308.

Azuma Y, Currie PJ. 2000. A new carnosaur (Dinosauria: Theropoda) from the Lower Cretaceous of Japan. *Canadian Journal of Earth Sciences* **37**: 1735–1753.

Barker CT, Hone DW, Naish D, Cau A, Lockwood JAF, Foster B, Clarkin CE, Schneider P, Gostling NJ. 2021. New spinosaurids from the Wessex Formation (Early Cretaceous, UK) and the European origins of Spinosauridae. *Scientific Reports* **11**: 19340.

Barker CT, Lockwood JA, Naish D, Brown S, Hart A, Tulloch E, Gostling NJ. 2022. A European giant: a large spinosaurid (Dinosauria: Theropoda) from the Vectis Formation (Wealden Group, Early Cretaceous), UK. *PeerJ* **10**: e13543.

Benson RB. 2010. A description of *Megalosaurus bucklandii* (Dinosauria: Theropoda) from the Bathonian of the UK and the relationships of Middle Jurassic theropods. *Zoological Journal of the Linnean Society* **158**: 882–935.

Beevor T, Quigley A, Smith RE, Smyth RS, Ibrahim N, Zouhri S, Martill DM. 2021. Taphonomic evidence supports an aquatic lifestyle for *Spinosaurus*. *Cretaceous Research* **117**: 104627.

Benson RB, Xing X. 2008. The anatomy and systematic position of the theropod dinosaur *Chilantaisaurus tashuikouensis* Hu, 1964 from the Early Cretaceous of Alanshan, People's Republic of China. *Geological Magazine* **145**: 778–789.

Bertin T. 2010. A catalogue of material and review of the Spinosauridae. *PalArch's Journal of Vertebrate Palaeontology* **7(4)**: 1–39.

Britt BB. 1991. Theropods of Dry Mesa Quarry (Morrison Formation, late Jurassic), Colorado, with emphasis on the osteology of *Torvosaurus tanneri*. *Brigham Young University Geology Studies* **37**: 1–72.

Brochu CA. 2003. Osteology of *Tyrannosaurus rex*: insights from a nearly complete skeleton and high-resolution computed tomographic analysis of the skull. *Journal of Vertebrate Paleontology* **22(4 suppl.)**: 1–138.

Buckland W. 1824. Notice on the *Megalosaurus* or great fossil lizard of Stonesfield. *Transactions of the Geological Society of London* **2(1)**: 390–396.

Buffetaut E. 2007. The spinosaurid dinosaur *Baryonyx* (Saurischia, Theropoda) in the Early Cretaceous of Portugal. *Geological Magazine* **144**: 1021–1025.

Buffetaut E, Ouaja M. 2002. A new specimen of *Spinosaurus* (Dinosauria, Theropoda) from the Lower Cretaceous of Tunisia, with remarks on the evolutionary history of the Spinosauridae. *Bulletin de la Société géologique de France* **173**: 415–421.

Buffetaut E, Martill D, Escuillié F. 2004. Pterosaurs as part of a spinosaur diet. *Nature* **430(6995)**: 33.

Burnham DA, Derstler KL, Currie PJ, Bakker RT, Zhou Z, Ostrom JH. 2000. Remarkable new birdlike dinosaur (Theropoda: Maniraptora) from the Upper Cretaceous of Montana. *University of Kansas Paleontological Contributions* **13**: 1–12.

Candeiro CRA, Brusatte SL, de Souza AL. 2017. Spinosaurid dinosaurs from the Early Cretaceous of North Africa and Europe: fossil record, biogeography and extinction. *Anuário do Instituto de Geociências* **40**: 294–302.

Canudo JI, Ruiz-Omeñaca JI. 2003. Los restos directos de dinosaurios terópodos (excluyendo Aves) en España. In: Pérez-Lorente F, Romero Molina MM, Rivas P, coords. *Dinosaurios y otros reptiles mesozoicos en España.* Ciencias de la Tierra 26. Logroño: Universidad de La Rioja, Instituto de Estudios Riojanos, 347–373.

Canudo JI, Gasulla JM, Ortega F, Ruiz-Omeñaca JI. 2004. Presencia de Baryonychinae (Theropoda) en el Aptiense inferior (Cretácico inferior) de Laurasia: Cantera Mas de la Parreta, Formación Arcillas de Morella (Morella, Castellón). In: Colectivo Arqueológico-Paleontológico de Salas, ed. Actas de las III Jornadas internacionales sobre Paleontología de Dinosaurios y su entorno. Salas de los Infantes: Colectivo Arqueológico y Paleontológico de Salas, 32–34.

Canudo JI, Gasulla JM, Gómez-Fernández D, Ortega F, Sanz JL, Yagüe P. 2008. Primera evidencia de dientes aislados atribuidos a Spinosauridae (Theropoda) en el Aptiano inferior (Cretácico Inferior) de Europa: formación Arcillas de Morella (España). *Ameghiniana* **45**: 649–652.

Carrano MT, Sampson SD. 2008. The phylogeny of Ceratosauria (Dinosauria: Theropoda). *Journal of Systematic Palaeontology* **6**: 183–236.

Carrano MT, Benson RB, Sampson SD. 2012. The phylogeny of Tetanurae (Dinosauria: Theropoda). *Journal of Systematic Palaeontology* **10**: 211–300.

Casas AM, Villalaín JJ, Soto R, Gil-Imaz A, Del Río P, Fernández G. 2009. Multidisciplinary approach to an extensional syncline model for the Mesozoic Cameros Basin (N Spain). *Tectonophysics* **470**: 3–20.

Casquet C, Galindo C, González-Casado JM, Alonso A, Mas R, Rodas M, García E, Barrenechea JF. 1992. El metamorfismo en la Cuenca de los Cameros. Geocronología e implicaciones tectónicas. *Geogaceta* **11:** 22–25.

Cerda IA, Chinsamy A, Pol D, Apaldetti C, Otero A, Powell JE, Martínez RN. 2017. Novel insight into the origin of the growth dynamics of sauropod dinosaurs. *PLoS ONE* **12(6):** e0179707.

Charig AJ, Milner AC. 1986. *Baryonyx*, a remarkable new theropod dinosaur. *Nature* **324**: 359–361.

Charig, AJ, Milner AC. 1997. *Baryonyx walkeri*, a fish-eating dinosaur from the Wealden of Surrey. *Bulletin of the Natural History Museum (Geology)* **53**: 11–70.

Chimsamy A, Raath MA. 1992. Preparation of fossil bone for histological examination. *Palaeontologia Africana* **29**: 39–44.

Clemente, P. 2010. Review of the Upper Jurassic-Lower Cretaceous stratigraphy in western Cameros basin, northern Spain. *Revista de la Sociedad Geológica de España* **23**: 101–143.

Company J. 2011. Bone histology of the titanosaur *Lirainosaurus astibiae* (Dinosauria: Sauropoda) from the latest Cretaceous of Spain. *Naturwissenschaften* **98:** 67–78.

Currie PJ, Zhao XJ. 1993. A new carnosaur (Dinosauria, Theropoda) from the Jurassic of Xinjiang, People's Republic of China. *Canadian Journal of Earth Sciences* **30**: 2037–2081.

Dal Sasso C, Maganuco S, Buffetaut E, Mendez MA. 2005. New information on the skull of the enigmatic theropod *Spinosaurus*, with remarks on its size and affinities. *Journal of Vertebrate Paleontology* **25**: 888–896.

Del Río P, Barbero L, Mata P, Fanning CM. 2009. Timing of diagenesis and very low-grade metamorphism in the eastern sector of the Sierra de Cameros (Iberian Range, Spain): a U–Pb SHRIMP study on monazite. *Terra Nova* **21:** 438–445.

D'Emic MD, O'Connor PM, Sombathy RS, Cerda I, Pascucci TR, Varricchio D, Pol D, Dave A, Coria RA, Curry-Rogers KA. 2023. Developmental strategies underlying gigantism and miniaturization in non-avialan theropod dinosaurs. *Science* **379:** 811–814.

Evers SW, Rauhut OW, Milner AC, McFeeters B, Allain R. 2015. A reappraisal of the morphology and systematic position of the theropod dinosaur *Sigilmassasaurus* from the "middle" Cretaceous of Morocco. *PeerJ* **3**: e1323.

Fabbri M, Navalón G, Benson RBJ, Pol D, O'Connor J, Bhullar B-AS, Erickson GM, Norell MA, Orkney A, Lamanna MC, Zouhri S, Becker J, Emke A, Dal Sasso C, Bindellini G, Maganuco S, Auditore M, Ibrahim N. 2022. Subaqueous foraging among carnivorous dinosaurs. *Nature* **603**: 852–857.

Francillon-Vieillot H, de Buffrénil V, Castanet J, Géraudie J, Meunier FJ, Sire JY, Zylerberg L, de Ricqlès A. 1990. Microstructure and mineralization of vertebrate skeletal tissues. In: Carter JG, ed. *Skeletal biomineralization: patterns, processes and evolutionary trends*, 1. New York: Van Nostrand Reinhold, 471–530.

de França TC, Santos Brilhante N, de Oliveira Monteiro Nobre Y, Medeiros MA, Matos Lindoso R, Rodrigues Costa F. 2021. The first record of a spinosaurid pedal ungual from Brazil (Boca do Forno Ravine, Itapecuru Formation, Parnaíba Basin). *Historical Biology* **34**: 1817–1826.

Figuereido S, Rosina P, Figuti L. 2015. Dinosaurs and other vertebrates from the Papo-Seco Formation (Lower Cretaceous) of southern Portugal. *Journal of Iberian Geology* **41**: 301–314.

Fuentes Vidarte C, Meijide Calvo M, Izquierdo LA, Montero D, Pérex G, Torcida F, Urién V, Meijide Fuentes F, Meijide Fuentes M. 2001. Restos fósiles de *Baryonyx* (Dinosauria, Theropoda) en el Cretácico inferior de Salas de los Infantes (Burgos, España). In: Colectivo Arqueológico-Paleontológico de Salas, ed. *Actas de las I Jornadas internacionales sobre Paleontología de Dinosaurios y su entorno*. Salas de los Infantes: Colectivo Arqueológico y Paleontológico de Salas, 349–359.

Galton PM, Jensen JA. 1979. A new large theropod dinosaur from the Upper Jurassic of Colorado. *Brigham Young University Geology Studies* **26**: 1–12.

Gasca JM, Moreno-Azanza M, Canudo JI. 2008. Dientes de dinosaurios terópodos espinosáuridos de la Formación El Castellar (Cretácico Inferior, Teruel). *Palaeontologica Nova* **8**: 233–234.

Gasca JM, Moreno-Azanza M, Canudo JI, 2011. Dientes de dinosaurios en el Barremiense de Allepuz, Teruel. In: Pérez-García A, Gascó F, Gasulla JM, Escaso F., eds. *Viajando a mundos pretéritos*. Morella: Ajuntament de Morella, 145–155.

Gasca JM, Díaz-Martínez I, Moreno-Azanza M, Canudo JI, Alonso A. 2018. A hypertrophied ungual phalanx from the lower Barremian of Spain: Implications for the diversity and palaeoecology of Spinosauridae (Theropoda) in Iberia. *Cretaceous Research* **84**: 141–152.

Gauthier JA. 1986. Saurischian monophyly and the origin of birds. In: Padian K., ed. The Origin of Birds and the Evolution of Flight. *Memoirs of the California Academy of Sciences* **8**: 1–55.

Gilmore CW. 1920. Osteology of the carnivorous Dinosauria in the United State National Museum: with special reference to the genera *Antrodemus* (*Allosaurus*) and *Ceratosaurus*. *Bulletin of the United States National Museum* **110**: 1–154.

Gilmore CW. 1933. On the dinosaurian fauna of the Iren Dabasu Formation. *Bulletin of the American Museum of Natural History* **67**: 23–95.

Goloboff PA, Catalano SA. 2016. TNT version 1.5, including a full implementation of phylogenetic morphometrics. *Cladistics* **32**: 221–238.

Goloboff PA, Farris S, Nixon K. 2008. TNT, a free programm for phylogenetic analysis. *Cladistics* **24**: 774–786.

Gordon AD. 1979. A measure of the agreement between rankings. *Biometrika* **66**: 7–15.

Gordon AD. 1980. On the assessment and comparison of classifications. In: Tomassone R, ed. *Analyse de donnés et informatique*. Le Chesnay: INRIA, 149–160.

Heckeberg NS, Rauhut OWM. 2020. Histology of spinosaurid dinosaur teeth from the Albian-Cenomanian of Morocco: implications for tooth replace ment and ecology. *Palaeontologia Electronica* **23(3)**: a48.

Hendrickx C, Mateus O, Araújo R. 2015. A proposed terminology of theropod teeth (Dinosauria, Saurischia). *Journal of Vertebrate Paleontology* **35**: e982797.

Hendrickx C, Mateus O, Araújo R, Choiniere J. 2019. The distribution of dental features in non-avian theropod dinosaurs: Taxonomic potential, degree of homoplasy, and major evolutionary trends. *Palaeontologia Electronica* **22.3.74**: 1–110.

Hendrickx C, Tschopp E, Ezcurra MD. 2020. Taxonomic identification of isolated theropod teeth: The case of the shed tooth crown associated with *Aerosteon* (Theropoda: Megaraptora) and the dentition of Abelisauridae. *Cretaceous Research* **108**: 104312.

Hernán FJ. 2018. Estratigrafía y sedimentología de las formaciones con icnitas de dinosaurios del Grupo Enciso (Cameros, La Rioja, Aptiense). PhD Thesis, Universidad Politécnica de Madrid.

Holtz TR, Molnar RE, Currie PJ. 2004. Basal Tetanurae. In: Weishampel DB, Dodson P, Osmólska H., eds., *The Dinosauria*, second ed. Berkeley: University of California Press, 71–110.

Hone DWE, Holtz TR Jr. 2017. A century of spinosaurs - A review and revision of the Spinosauridae with comments on their ecology. *Acta Geologica Sinica-English Edition* **91**: 1120–1132.

Hone DWE, Holtz TR. 2021. Evaluating the ecology of *Spinosaurus*: shoreline generalist or aquatic pursuit specialist? *Palaeontologia Electronica* **24**: 1–28.

Hu SY. 1964. [Carnosaurian remains from Alashan, Inner Mongolia]. *Vertebrata PalAsiatica* **8**: 42–63 (In Chinese).

Hutchinson JR. 2001. The evolution of pelvic osteology and soft tissues on the line to extant birds (Neornithes). *Zoological Journal of the Linnean Society* **131**: 123–168.

Ibrahim N, Sereno PC, Dal Sasso C, Maganuco S, Fabbri M, Martill DM, Zouhri S, Myhrvold N, Iurino DA. 2014. Semiaquatic adaptations in a giant predatory dinosaur. *Science* **345**: 1613–1616.

Ibrahim N, Maganuco S, Dal Sasso C, Fabbri M, Auditore M, Bindellini G, Martill DV, Zouhri S, Mattarelli DA, Unwin DM, Wiemann J, Bonadonna D, Amane A, Jakubczak J, Joger U, Lauder GV, Pierce SE. 2020. Tail-propelled aquatic locomotion in a theropod dinosaur. *Nature* **581(7806)**: 67–70.

Infante P, Canudo JI, Ruiz-Omeñaca JI. 2005. First evidence of theropod dinosaurs from the Mirambel Formation (Lower Barremian, Lower Cretaceous) from Castellote, Teruel. *Geogaceta* **38**: 31–34.

Isasmendi E, Sáez-Benito P, Torices A, Navarro-Lorbés P, Pereda-Suberbiola X. 2020. New insights about theropod palaeobiodiversity in the Iberian Peninsula and Europe: Spinosaurid teeth (Theropoda, Megalosauroidea) from the Lower Cretaceous of La Rioja (Spain). *Cretaceous Research* **116**: 104600.

Isasmendi E, Navarro-Lorbés P, Sáez-Benito P, Viera LI, Torices A, Pereda-Suberbiola X. 2023. New contributions to the skull anatomy of spinosaurid theropods: Baryonychinae maxilla from the Early Cretaceous of Igea (La Rioja, Spain). *Historical Biology* online: 1-15 (DOI 10.1080/08912963.2022.2069019).

Kellner AW, Campos DDA. 1996. First Early Cretaceous theropod dinosaur from Brazil with comments on Spinosauridae. *Neues Jahrbuch für Geologie und Paläontologie Abhandlungen* **199**: 151–166.

Kellner AW, Azevedo SA, Machado EB, Carvalho LBD, Henriques DD. 2011. A new dinosaur (Theropoda, Spinosauridae) from the Cretaceous (Cenomanian) Alcântara Formation, Cajual Island, Brazil. *Anais da Academia Brasileira de Ciências* **83**: 99–108.

Lacerda MBS, Aragão PRL, Vieira FS, Sales MAF, Liparini A. 2023. On the first Baryonychinae (Theropoda, Spinosauridae) teeth from South America. *Zootaxa* **5264**: 526–544

Lamm ET. 2013. Preparation and sectioning of specimens. In: Padian K, Lamm ET, eds. *Bone Histology of Fossil Tetrapods: Advancing Methods, Analysis and Interpretation*. Berkeley: University of California Press, 55–160.

Maddison WP, Maddison DR. 2008. Mesquite: A modular system for evolutionary analysis. *Evolution* **62**: 1103–1118.

Mader BJ, Bradley RL. 1989. A redescription and revised diagnosis of the syntypes of the Mongolian tyrannosaur *Alectrosaurus olseni*. *Journal of Vertebrate Paleontology* **9**: 41–55.

Maganuco S, Dal Sasso C. 2018. The smallest biggest theropod dinosaur: a tiny pedal ungual of a juvenile *Spinosaurus* from the Cretaceous of Morocco. *PeerJ* **6**: e4785.

Malafaia E, Ortega F, Escaso F, Mocho P. 2013. Rediscovery of a lost portion of the holotype of *Suchosaurus girardi* (Sauvage, 1897–98), now related to the spinosaurid theropod *Baryonyx*. In: Torcida Fernández-Baldor F., Huerta P, eds. *Actas de las VI Jornadas Internacionales sobre Dinosaurios y su entorno*. Salas de los Infantes: Colectivo Arqueológico-Paleontológico de Salas, 82–84.

Malafaia E, Gasulla JM, Escaso F, Narváez I, Sanz JL, Ortega F. 2018. New spinosaurid (Theropoda, Megalosauroidea) remains from the Arcillas de Morella Formation (upper Barremian) of Morella, Spain. *Cretaceous Research* **92**: 174–183.

Malafaia E, Mocho P, Escaso F, Dantas P, Ortega F. 2019. Carcharodontosaurian remains (Dinosauria, Theropoda) from the Upper Jurassic of Portugal. *Journal of Paleontology* **93**: 157–172.

Malafaia E, Gasulla JM, Escaso F, Narváez I, Sanz JL, Ortega F. 2020a. A new spinosaurid theropod (Dinosauria: Megalosauroidea) from the upper Barremian of Vallibona, Spain: Implications for spinosaurid diversity in the Early Cretaceous of the Iberian Peninsula. *Cretaceous Research* **106**: 104221.

Malafaia E, Gasulla JM, Escaso F, Narvaéz I, Ortega F. 2020b. An update of the spinosaurid (Dinosauria: Theropoda) fossil record from the Lower Cretaceous of the Iberian Peninsula: distribution, diversity, and evolutionary history. *Journal of Iberian Geology* **46**: 431–444.

Marsh OC. 1877. Notice of some new dinosaurian reptiles from the Jurassic Formation. *American Journal of Science* (ser. 3) **14**: 514–516.

Marsh OC. 1881. Principal characters of American Jurassic dinosaurs, part V. *American Journal of Science* (ser. 3) **21**: 417–423.

Martill DM, Cruickshank ARI, Frey E, Small PG, Clarke M. 1996. A new crested maniraptoran dinosaur from the Santana Formation (Lower Cretaceous) of Brazil. *Journal of the Geological Society* **153**: 5–8.

Martín-Chivelet J, López-Gómez J, Aguado R, Arias C, Arribas J, Arribas ME, Aurell M, Bádenas B, Benito MI, Bover-Arnal T, Casas-Sainz A, Castro JM, Coruña F., de Gea GA, Fornós JJ, Fregenal-Martínez M, García-Senz J, Garófano D, Gelabert B, Giménez J, González-Acebrón J, Guimerà J, Liesa CL, Mas R, Meléndez N, Molina JM, Muñoz JA, Navarrete R, Nebot M, Nieto LM, Omodeo-Salé S, Pedrera A, Peropadre C, Quijada IE, Quijano ML, Reolid M, Robador A, Rodríguez-López JP, Rodríguez-Perea A, Rosales I, Ruiz-Ortiz PA, Sàbat F, Salas R, Soria AR, Suarez-Gonzalez P, Vilas L. 2019. The Late Jurassic–Early Cretaceous Rifting. In: Quesada C, Oliveira JT, eds. *The Geology of Iberia: A Geodynamic Approach*, vol. 3: The Alpine Cycle. Heidelberg: Springer, 169–249.

Martín-Closas C, Alonso Millán A. 1998. Estratigrafía y bioestratigrafía (Charophyta) del Cretácico Inferior en el sector occidental de la Cuenca de Cameros (Cordillera Ibérica). *Revista de la Sociedad Geológica de España* **11**: 253–270.

Mas JR, Alonso A, Guimerá J. 1993. Evolución tectonosedimentaria de una cuenca extensional intraplaca: la cuenca finijurásica-eocretácica de Los Cameros (La Rioja-Soria). *Revista de la Sociedad Geológica de España* **6**: 129–144.

Mas R, Benito MI, Arribas J, Serrano A, Guimerà J, Alonso Á, Alonso-Azcárate J. 2002. La Cuenca de Cameros: desde la extensión finijurásica-eocretácica a la inversión terciaria - Implicaciones en la exploración de hidrocarburos. *Zubía Monográfico* **14**: 9–64.

Mas R, Benito MI, Arribas J, Alonso Á., Arribas ME, Lohmann KC, González-Acebrón L, Hernán J, Quijada E, Suarez P., Omodeo S. 2011. Evolution of an intra-plate rift basin: the Latest Jurassic-Early Cretaceous Cameros Basin (Northwest Iberian Ranges, North Spain). In: Arenas C, Pomar L, Colombo F, eds. *Post-Meeting Field Trips, 28th IAS Meeting Zaragoza*. Geo-Guías 8. Zaragoza: Sociedad Geológica de España, 117–154.

Mata MP, Casas AM, Canals A, Gil A, Pocovi A. 2001. Thermal history during Mesozoic extension and Tertiary uplift in the Cameros Basin, northern Spain. *Basin Research* **13**: 91–111.

Mateus O, Estraviz-López D. 2022. A new theropod dinosaur from the Early Cretaceous (Barremian) of Cabo Espichel, Portugal: Implications for spinosaurid evolution. *PLoS ONE* **17**: e0262614.

Mateus O, Araújo R, Natário C, Castanhinha R. 2011. A new specimen of the theropod dinosaur *Baryonyx* from the Early Cretaceous of Portugal and taxonomic validity of *Suchosaurus*. *Zootaxa* **2827**: 54–68.

Meyer H von. 1832. Paleologica zur Geschichte der Erde. Frankfurt am Main: S. Schmerber.

Milner AC. 2003. Fish-eating theropods: a short review of the systematics, biology and palaeobiology of spinosaurs. In: Colectivo Arqueológico-Paleontológico de Salas, ed. *Actas de las II Jornadas internacionales sobre Paleontología de Dinosaurios y su entorno*. Salas de los Infantes: Colectivo Arqueológico y Paleontológico de Salas, 129–139.

Norell MA, Clark JM, Makovicky PJ. 2001. Phylogenetic relationships among coelurosaurian theropods. In: Gauthier J, Gall LF, eds. New Perspectives on the Origin and Early Evolution of Birds. New Haven: Yale Peabody Museum, 49–67.

Novas F, Dalla Vecchia F, Pais D. 2005. Theropod pedal unguals from the Late Cretaceous (Cenomanian) of Morocco, Africa. *Revista del Museo Argentino de Ciencias Naturales* **7**: 167–175.

Omodeo-Salé S, Salas R, Guimerá J, Ondrak R, Mas R, Arribas J, Suárez-Ruiz I, Martinez L. 2017. Subsidence and thermal history of an inverted Late Jurassic-Early Cretaceous extensional basin (Cameros, North-central Spain) affected by very low- to low-grade metamorphism. *Basin Research* **29:** 156–174.

Osborn HF. 1905. *Tyrannosaurus* and other Cretaceous carnivorous dinosaurs. *Bulletin of the American Museum of Natural History* **21**: 259–265.

Ostrom JH. 1969. A new theropod dinosaur from the Lower Cretaceous of Montana. *Postilla* **128**: 1–17.

Owen R. 1842. Report on British Fossil Reptiles. Part II. *Reports of the British Association for the Advancement of Science* **1841**: 60–204.

Pereda-Suberbiola X, Torcida F, Izquierdo LA, Huerta P, Montero D, Pérez G. 2003. First rebbachisaurid dinosaur (Sauropoda, Diplodocoidea) from the early Cretaceous of Spain: palaeobiogeographical implications. *Bulletin de la Société géologique de France* **174**: 471–479.

Pol D, Escapa IH. 2009. Unstable taxa in cladistic analysis: identification and the assessment of relevant characters. *Cladistics* **25**: 515–527.

Rauhut OWM. 2003. The Interrelationships and Evolution of Basal Theropod Dinosaurs. *Special Papers in Palaeontology* **69**: 1–213.

Rauhut OWM 2005. Osteology and relationships of a new theropod dinosaur from the Middle Jurassic of Patagonia. *Palaeontology* **48**: 87–110.

Rauhut OWM, Pol D. 2019. Probable basal allosauroid from the early Middle Jurassic Cañadón Asfalto Formation of Argentina highlights phylogenetic uncertainty in tetanuran theropod dinosaurs. *Scientific Reports* **9**: 1–9.

Rauhut OWM, Pol D. 2021. New theropod remains from the Late Jurassic Cañadón Calcáreo Formation of Chubut, Argentina. *Journal of South American Earth Sciences* **111**: 103434.

Rauhut OWM, Hübner TR, Lanser K-P. 2016. A new megalosaurid theropod dinosaur from the late Middle Jurassic (Callovian) of north-western Germany: Implications for theropod evolution and faunal turnover in the Jurassic. *Palaeontologia Electronica* **19.2.26A**: 1–65.

Rauhut OWM, Canudo JI, Castanera D. 2019. A reappraisal of the Early Cretaceous theropod dinosaur *Camarillasaurus* from Spain. In: *17th Conference of the European Association of Vertebrate Palaeontologists (EAVP)*, Program and Abstracts, Brussels, 96.

Ruiz-Omeñaca JI. 2006. Restos directos de dinosaurios (Saurischia, Ornithischia) en el Barremiense (Cretácico Inferior) de la Cordillera Ibérica en Aragón (Teruel, España). PhD Thesis, Universidad de Zaragoza.

Ruiz-Omeñaca JI, Canudo JI, Cuenca-Bescós G. 1996. Dientes de dinosaurios (Ornithischia, Saurischia) del Barremiense superior (Cretácico inferior) de Vallipón (Castellote, Teruel). *Mas de las Matas* **15**: 59–103.

Ruiz-Omeñaca JI, Canudo JI, Cuenca-Bescós G. 1998. Primera cita de dinosaurios barionícidos (Saurischia: Theropoda) en el Barremiense superior (Cretácico Inferior) de Vallipón (Castellote, Teruel). *Mas de las Matas* **17**: 201–223.

Ruiz-Omeñaca JI, Cruzado-Caballero P, Infante P, Moreno-Azanza M. 2005. Baryonychine teeth (Theropoda: Spinosauridade) from the Lower Cretaceous of La Cantalera (Josa, NE Spain). *Kaupia* **14**: 59–63.

Russell DA. 1996. Isolated Dinosaur bones from the Middle Cretaceous of the Tafilalt, Morocco. *Bulletin du Muséum National d'histoire Naturelle* (ser. 4 C) **18**: 349–402

Sales M A, Schultz CL. 2017. Spinosaur taxonomy and evolution of craniodental features: Evidence from Brazil. *PLoS ONE*, **12(11)**: e0187070.

Sales MA, Lacerda MB, Horn BL, de Oliveira, IA, Schultz CL. 2016. The "χ" of the matter: testing the relationship between paleoenvironments and three theropod clades. *PLoS ONE* **11(2)**: e0147031.

Samathi A, Sander PM, Chanthasit P. 2021. A spinosaurid from Thailand (Sao Khua Formation, Early Cretaceous) and a reassessment of *Camarillasaurus cirugedae* from the Early Cretaceous of Spain. *Historical Biology* **33**: 3480–3494.

Sánchez-Hernández B, Benton MJ. 2014. Filling the ceratosaur gap: A new ceratosaurian theropod from the Early Cretaceous of Spain. *Acta Palaeontologica Polonica* **59**: 581–600.

Sánchez-Hernández B, Benton MJ, Naish D. 2007. Dinosaurs and other fossil vertebrates from the Late Jurassic and Early Cretaceous of the Galve area, NE Spain. *Palaeogeography, Palaeoclimatology, Palaeoecology* **249**: 180–215.

Santos-Cubedo A, de Santisteban C, Poza B, Meseguer S. 2023. A new spinosaurid dinosaur species from the Early Cretaceous of Cinctorres (Spain). *Scientific Reports* **13(1)**: 6471.

Schade M, Rauhut OWM, Foth C, Moleman O, Evers SW. 2023. A reappraisal of the cranial and mandibular osteology of the spinosaurid *Irritator challengeri* (Dinosauria: Theropoda). *Palaeontologia Electronica* **26(2)**: a17.

Schudack U, Schudack M. 2009. Ostracod biostratigraphy in the Lower Cretaceous of the Iberian chain (Eastern Spain). *Journal of Iberian Geology* **35**: 141–168.

Sereno PC, Wilson JA, Larsson HCE, Dutheil DB, Sues, H-D. 1994. Early Cretaceous dinosaurs from the Sahara. *Science* **266**: 267–270.

Sereno PC, Dutheil DB, Iarochene M, Larsson HCE, Lyon GH, Magwene PM, Sidor CA, Varricchio DJ, Wilson JA. 1996. Predatory dinosaurs from the Sahara and Late Cretaceous faunal differentiation. *Science* **272**: 986–991.

Sereno PC, Beck AL, Dutheil DB, Larsson HCE, Lyon GH, Marcot JD, Rauhut OWM, Sadleir RW, Sidor CA, Varricchio DD, Wilson GP, Wilson JA. 1998. A long-snouted predatory dinosaur from Africa and the evolution of Spinosaurids. Science **282**: 1298–1302.

Sereno PC, Wilson JA, Conrad J L. 2004. New dinosaurs link southern landmasses in the Mid–Cretaceous. *Proceedings of the Royal Society of London* B **1546**: 1325–1330.

Sereno PC, Myhrvold N, Henderson DM, Fish FE, Vidal D, Baumgart S. L., Keillor TM, Formoso KK, Conroy LL. 2022. *Spinosaurus* is not an aquatic dinosaur. *eLife* **11**: e80092.

Stromer E. 1915. Ergebnisse der Forschungsreisen Prof. E. Stromers in den Wüsten Ägyptens. II. Wirbeltier-Reste der Baharîje-Stufe (unterstes Cenoman). 3. Das Original des Theropoden *Spinosaurus aegyptiacus* nov. gen., nov. spec. *Abhandlungen der Königlich Bayerischen Akademie der Wissenschaften, Mathematisch-physikalische Klasse* **28**: 1–32.

Stromer E. 1934. Ergebnisse der Forschungsreisen Prof. E. Stromers in den Wüsten Ägyptens. II. Wirbeltierreste der Baharîje-Stufe. 13 Dinosauria. *Abhandlungen der Bayerischen Akademie der Wissenschaften, Mathematisch-Naturwissenschaftliche Abteilung* **22**: 1–79.

S**uarez-Gonzalez P, Quijada IE, Benito Moreno MI, Mas Mayoral JR. 2013.** Eustatic versus tectonic control in an intraplate rift basin (Leza Fm, Cameros Basin). Chronostratigraphic and paleogeographic implications for the Aptian of Iberia. *Journal of Iberian Geology* **39**: 285–312.

Suarez-Gonzalez P, Quijada IE, Benito MI, Mas R. 2015. Sedimentology of ancient coastal wetlands: insights from a Cretaceous multifaceted depositional system. *Journal of Sedimentary Research* **85**: 95–117.

Taquet P, Russell DA. 1998. New data on spinosaurid dinosaurs from the Early Cretaceous of the Sahara. *Comptes Rendus de l'Académie des Sciences* (IIA) **327**: 347–353.

Tischer G. 1966. Über die Wealden-Ablagerung und die tektonik der östlichen Sierra de los Cameros in den nordwestlichen Iberischen Ketten (Spanien). *Beihefte zum Geologischen Jahrbuch* **44**: 123–164.

Torcida F, Fuentes C, Izquierdo LA, Montero DM, Urién V. 1997. Dientes de dinosaurios terópodos (cf. *Baryonyx*) en el Weald de Burgos (España). *Stvdia Geologica Salmanticensia* **33**: 59–65.

Torcida Fernández-Baldor F, Izquierdo Montero LA, Huerta Hurtado P, Montero Huerta D, Pérez Martínez G. 2003. Dientes de dinosaurios (Theropoda, Sauropoda), en el Cretácico

Inferior de Burgos (España). In: Pérez-Lorente F, Romero Molina MM, Rivas P, coords. *Dinosaurios y otros reptiles mesozoicos en España.* Ciencias de la Tierra 26. Logroño: Universidad de La Rioja, Instituto de Estudios Riojanos, 335–346.

Viera LI, Torres JA. 2013. *La Rioja de los Dinosaurios: un ecosistema de hace 120 millones de años*. Igea: Sociedad de Ciencias Aranzadi, Centro de Interpretación Paleontológica de La Rioja, 1–136.

Walker AD. 1964. Triassic reptiles from the Elgin area: *Ornithosuchus* and the origin of carnosaurs. *Philosophical Transactions of the Royal Society of Londo*n B **248**: 53–134.

Wang S, Stiegler J, Amiot R, Wang X, Du G, Clark JM, Xu X. 2017. Extreme ontogenetic changes in a ceratosaurian theropod. *Current Biology* **27**: 144–148.

Figure 1. Geographical and geological location of northeastern Cameros Basin. A, geological map showing the location of Virgen del Villar-1 site in Igea (La Rioja, Spain) (modified from Suarez-Gonzalez *et al.*, 2013). B, geographical map of the Iberian Peninsula.

Figure 2. Skeletal reconstruction of *Riojavenatrix lacustris* holotype recovered at Virgen del Villar - 1 site (La Rioja, Spain). The preserved material is coloured in fuchsia. Courtesy of Scott Hartman.

Figure 3. *Riojavenatrix lacustris* gen. et sp. nov., mid- to posterior dorsal vertebra (CPI 1677). A, anterior view. B, left lateral view. C, posterior view. Abbreviations: hy, hyposphene; ils, interspinous ligament scar; nc, neural canal; ns, neural spine; pcdl, posterior centrodiapophyseal lamina; pocdp, postzygocentrodiapophyseal fossa; sdf, spinodiapophyseal fossa; spof, spinopostzygapophyseal fossa; spol, spinopostzygapophyseal laminae; sprf; spinoprezygapophyseal fossa; sprl, spinoprezygapophyseal laminae; tp, transverse process. Scale bar equals 5 cm.

Figure 4. *Riojavenatrix lacustris* gen. et sp. nov., left pubis (CPI 1675A–B) and right ischium (CPI 1641A–B) in anterior (A, F, K, O), medial (B, G, L, P), lateral (C, I, M, R), posterior (D, J, N, S), proximal (E, Q) and distal (H, T) views. A–E, proximal left pubis. F–J, left pubic shaft and distal boot. K–N, proximal right ischium. O–T, right ischial shaft and distal boot. Abbreviations: ap, anterior process of the ischial boot; as, acetabular surface; ilp, iliac peduncle; isb, ischial boot; isp, ischial peduncle; on, obturator notch; pa, pubic apron; pb, pubic boot; pbg, posterior bulge. Scale bars equal 5 cm.

Figure 5. *Riojavenatrix lacustris* gen. et sp. nov., left (CPI 1637) and right (CPI 1643) femora in anterior (A, E), lateral (B, F), posterior (C, G), medial (D, H), distal (I) and proximal (J) views. A–D and J, proximal right femur. E–I, shaft and distal epiphysis of the left femur. Abbreviations: fh, femoral head; ctf, crista tibiofibularis; exg, extensor groove; ft, fourth trochanter; fxg, flexor groove; gt, greater trochanter, lc, lateral condyle; me, medial epicondyle; mc, medial condyle; pag, proximal articular groove. Scale bars equal 10 cm.

Figure 6. *Riojavenatrix lacustris* gen. et sp. nov., right tibia (CPI 1642), left tibia and astragalus (CPI 1638), and left fibula (CPI 1639A–B) in anterior (A, E, K, P), lateral (B, F, L, Q), posterior (C, G, M, R), medial (D, H, N, S), proximal (I, J, O) and distal (T). A–D and I, proximal end of the right tibia. E–H and J, left tibia and astragalus. K–O, shaft and proximal end of the left fibula. P–T, distal end of the left fibula. Abbreviations: asf, astragalar facet; ast, astragalus; cn, cnemial crest; fc, fibular crest; icn, intercondylar notch; ift, iliofibularis tubercle; it, incisura tibialis; lc, lateral condyle; lm, lateral malleolus; mf, medial fossa; mm, medial malleolus; sab, supraastragalar buttress. Scale bars equal 10 cm for A–O and 5 cm for P–T.

Figure 7. *Riojavenatrix lacustris* gen. et sp. nov., left astragalus and distal tibia (CPI 1638), and left calcaneum (CPI 1676) in anterior (A, H), lateral (B, I), posterior (C, J), medial (D, K), proximal (F) and distal (G). Abbreviations: af, astragalar facet; ag, anterior groove; apa, ascending process of the astragalus; ff, fibular facet; fo, foramen; lc, lateral condyle; mc, medial condyle; r, ridge; tf, tibial facet; vg, ventral groove. Scale bars equal 5 cm.

Figure 8. *Riojavenatrix lacustris* gen. et sp. nov., left pedal elements. Metatarsal III (CPI 1640), I-2 phalanx (CPI 1647), phalanx III-1 (CPI 1645), phalanx III-3 (CPI 1646) and phalanx V-2 (or IV-3) (CPI 1648) in distal (A, L, R), dorsal (B, G, M, S, X), lateral (C, H, N, T, Y), ventral (D, I, P, V, AA), medial (E, J, Q, W, AB) and proximal (F, K, O, U, Z). A–F, left metatarsal III. G–K, left pedal phalanx I-2. L–Q, left pedal phalanx III-1. R–W, left pedal phalanx III-3. X–AB, left pedal phalanx V-2 (or IV-3). Abbreviations: ft, flexor tuberosity; ef, extensor fossa; k, keel; lc, lateral condyle; lclp, lateral collateral ligament pit; lg, longitudinal groove; lpvf; lateral proximoventral fossa; mc, medial condyle; mclp, medial collateral ligament pit; mpvf; medial proximoventral fossa; pdl, proximodorsal lip. Scale bars equal 5 cm.

Figure 9. Phylogenetic results showing the phylogenetic position of *Riojavenatrix* based on the matrix of Rauhut & Pol (2021). Reduced consensus by iterPCR obtained from the 10000 MPTs. Alternative placements of *Riojavenatrix* and other pruned taxa are indicated by letters and indicated in the legends (right up). The coloured nodes indicate the main clades (legends in left down).

Figure 10. Phylogenetic results showing the phylogenetic position of *Riojavenatrix* based on the matrix of Mateus & Estraviz-López (2022). A. Strict consensus obtained from 307 MPTs. Bremer support values are up to the nodes, and Jackknife and bootstrap values are down to the nodes. B.

Reduced consensus by agreement subtree methodology with 16 taxa, Jackknife and bootstrap values are down to the nodes. The coloured nodes indicate the main clades (legends in left down).

Figure 11. Comparison of spinosaurid elements with *Riojavenatrix lacustris* gen. et sp. nov. (A) left pubic boot of *Riojavenatrix* (CPI 1675A–B), (B) right pubic boot of *Ichthyovenator* (DMS BK10-11; based on Allain *et al.*, 2012), (C) left pubic boot of *Baryonyx* (NHMUK VP R9951), (D) left pubic boot of *Suchomimus* (MNN GDF500), and (E) right pubic boot of FSAC-KK 11888 in distal view. (F) right ischial boot of *Riojavenatrix* (CPI 1641A–B), (G) right ischial boot of *Vallibonavenatrix* (MSMCa-1–3), (H) left ischial boot of *Suchomimus* (MNN GDF500), (I) left ischial boot of FSAC-KK 11888, and (J) right ischial boot of *Ichthyovenator* (DMS BK10-13; based on Allain *et al.*, 2012) in lateral view. Note that the drawing of the pubic boot of *Ichthyovenator* (DMS BK10-11) and FSAC-KK 11888, and the ischial boot of *Suchomimus* (MNN GDF500) is a mirror image of the element. Note that the arrows point anteriorly. Scale bars equal 5 cm.

Figure 12. Comparison of spinosaurid elements with *Riojavenatrix lacustris* gen. et sp. nov. Megalosauroid femora in (A–F) distal and (G–J) proximal views. Left femur of (A) *Riojavenatrix* (CPI 1637), (E, J) *Suchomimus* (MNN GDF500) and (I) *Baryonyx* (NHMUK VP R9951), and right femur of (B) CMP-2b/21, (C) *Megalosaurus* (NHMUK PV 31806), (D) *Baryonyx* (NHMUK VP R9951), (F) FSAC-KK 11888, (G) *Riojavenatrix* (CPI 1643) and (H) CMP-MS-0/22. Abbreviations; fh, femoral head; cft, crita tibiofibularis; exg, extensor groove; fxg, flexor groove; gt, greater trochanter; lc, lateral condyle; mc, medial condyle; pag, proximal articular groove. Note that the drawings of *Baryonyx* (NHMUK VP R9951), *Suchomimus* (MNN GDF500) in proximal view, and *Baryonyx* (NHMUK VP R9951), *Megalosaurus* (NHMUK PV 31806), CMP-2b/211 and FSAC-KK 11888 are mirror images of the elements. Scale bars equal 5 cm.

Figure 13. Comparison of spinosaurid elements with *Riojavenatrix lacustris* gen. et sp. nov. Left tibia of (A) *Riojavenatrix* (CPI 1638) and (D) *Suchomimus* (MNN GDF500), and right tibia of (B) *Riojavenatrix* (CPI 1642), (C) *Camarillasaurus* (MPG-KPC8) and (E) FSAC-KK 11888 in proximal view. Abbreviations: cn, cnemial crest; icn, intercondylar notch; it, incisura tibialis; lc, lateral condyle; mc, medial condyle. Note that the drawings of *Camarillasaurus* (MPG-KPC8), *Riojavenatrix* (CPI 1638) and FSAC-KK 11888 are mirror images of the elements. Scale bars equal 10 cm.

Figure 14. Comparison of spinosaurid elements with *Riojavenatrix lacustris* gen. et sp. nov. Left calcaneum of (A) *Riojavenatrix* (CPI 1676) and (B) *Iberospinus* (ML1190-31; based on Mateus & Estraviz-López, 2022), and right calcaneum of (C) *Baryonyx* (NHMUK VP R9951) in lateral view. Abbreviations: ff, fibular facet; fo, foramen. Note that the drawing of *Baryonyx* (NHMUK VP R9951) is a mirror image of the element. Scale bars equal 5 cm.

Figure 15. Comparison of spinosaurid elements with *Riojavenatrix lacustris* gen. et sp. nov. Left I-2 pedal phalanx of (A) *Riojavenatrix* (CPI 1647) and (F) *Deinonychus* (YPM 5205), and right I-2 pedal phalanx of (B) Carcharodontosauria indeterminate (SHN.019), (C) *Tyrannosaurus* (FMNH PR2081; based on Brochu, 2003), (D) *Bambiraptor* (AMNH 30556) and (E) *Alectrosaurus* (AMNH 6554) in medial view. Abbreviations: lg, longitudinal groove. Note that the drawing of *Alectrosaurus* (AMNH 6554), *Bambiraptor* (AMNH 30556), *Tyrannosaurus* (FMNH PR2081) and the indeterminate carcharodontosaurian (SHN.019) are mirror images of the elements. Scale bars equal 2 cm, but for D, which is 1 cm.

Figure 16. Histological preparations of *Riojavenatrix lacustris* gen. et sp. nov. material. A, polished cross-section of a possible fragment of the proximal right femur (CPI 1643) in ventral view, showing a thin cortex enclosing a medullary cavity invaded by bony trabeculae of cancellous bone. B, transverse polished section of a fragmentary vertebral centrum showing an internal pneumatized

internal structure. Note the presence of a couple of lines of arrested growth visible even to the naked eye (blue arrowheads). C, transverse thin section of the cortical bone of the same specimen, showing a clear pattern of stratification produced by the cyclical presence of lines of arrested growth (blue arrowheads). D, transverse thin section of the externalmost cortex of a fragmentary dyaphyseal limb bone fragment, showing two well-preserved lines of arrested grow (blue arrowheads), several isolated secondary osteons and oval erosion rooms (note that these resorption cavities are surrounded only by a single coat of lamellar bone tissue, remaining as open, incipient secondary osteons). Bone surface is on the top. E, same thin section showing intense remodelation in the internalmost cortex. Only two generations of secondary osteons are observed. Although densely packed, secondary osteons overlap each other very little. Abbreviations: pc, pneumatic cavity; Q, quartz cement; er, erosion room; so, secondary osteons. Photographs B–D in plane polarized light. Scale bars equal 1 cm for A, 0.1 mm in B and C, and 1 mm in D.

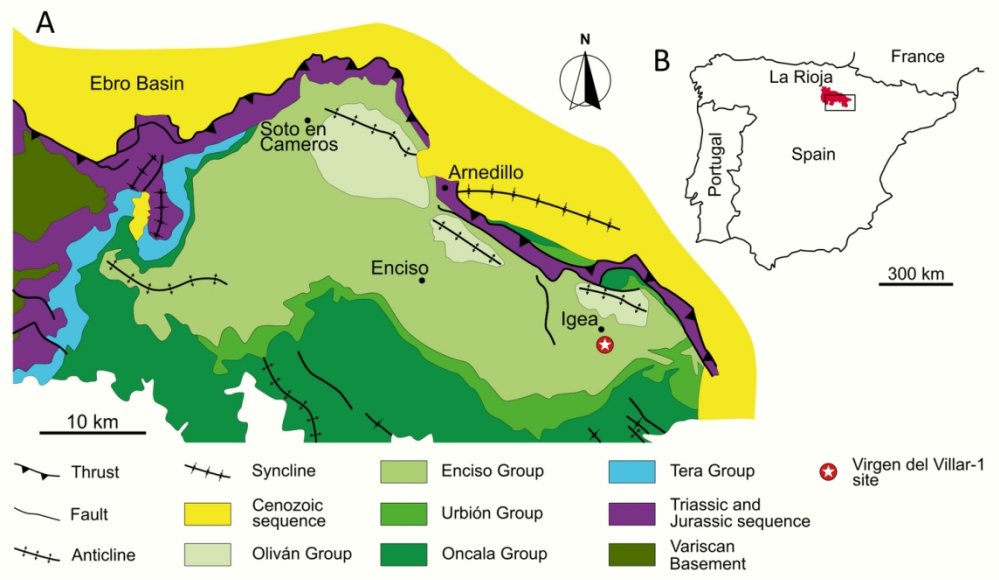

Figure 1. Geographical and geological location of northeastern Cameros Basin. A, geological map showing the location of Virgen del Villar-1 site in Igea (La Rioja, Spain) (modified from Suarez-Gonzalez et al., 2013). B, geographical map of the Iberian Peninsula.

62x36mm (600 x 600 DPI)

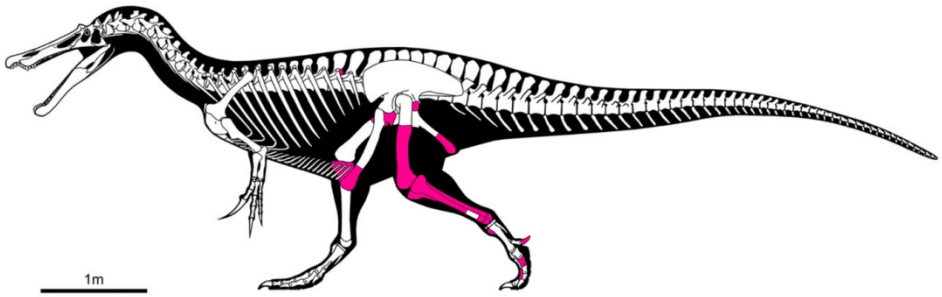

Figure 2. Skeletal reconstruction of *Riojavenatrix lacustris* holotype recovered at Virgen del Villar -1 site (La Rioja, Spain). The preserved material is coloured in fuchsia. Courtesy of Scott Hartman.

63x20mm (600 x 600 DPI)

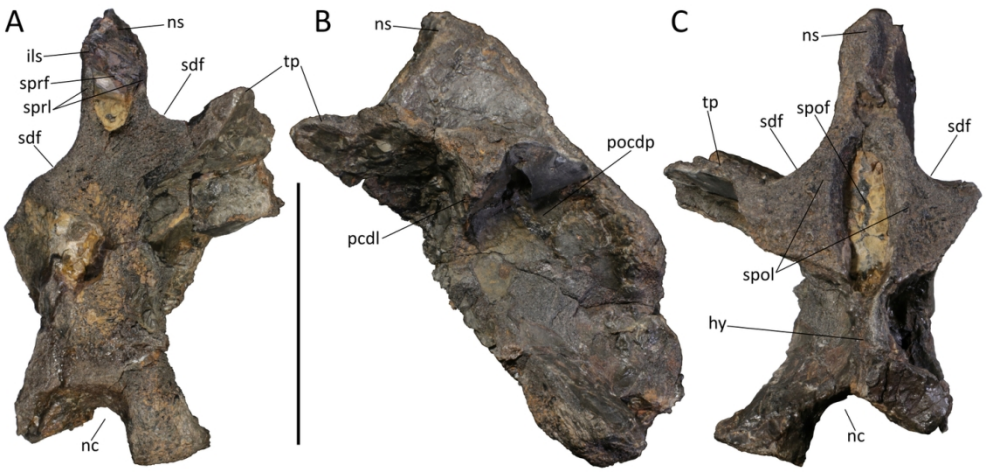

Figure 3. *Riojavenatrix lacustris* gen. et sp. nov., mid- to posterior dorsal vertebra (CPI 1677). A, anterior view. B, left lateral view. C, posterior view. Abbreviations: hy, hyposphene; ils, interspinous ligament scar; nc, neural canal; ns, neural spine; pcdl, posterior centrodiapophyseal lamina; pocdp, postzygocentrodiapophyseal fossa; sdf, spinodiapophyseal fossa; spof, spinopostzygapophyseal fossa; spol, spinopostzygapophyseal laminae; sprf; spinoprezygapophyseal fossa; sprl, spinoprezygapophyseal laminae; tp, transverse process. Scale bar equals 5 cm.

62x30mm (600 x 600 DPI)

Figure 4. *Riojavenatrix lacustris* gen. et sp. nov., left pubis (CPI 1675A–B) and right ischium (CPI 1641A–B) in anterior (A, F, K, O), medial (B, G, L, P), lateral (C, I, M, R), posterior (D, J, N, S), proximal (E, Q) and distal (H, T) views. A–E, proximal left pubis. F–J, left pubic shaft and distal boot. K–N, proximal right ischium. O–T, right ischial shaft and distal boot. Abbreviations: ap, anterior process of the ischial boot; as, acetabular surface; ilp, iliac peduncle; isb, ischial boot; isp, ischial peduncle; on, obturator notch; pa, pubic apron; pb, pubic boot; pbg, posterior bulge. Scale bars equal 5 cm.

62x81mm (600 x 600 DPI)

Figure 5. *Riojavenatrix lacustris* gen. et sp. nov., left (CPI 1637) and right (CPI 1643) femora in anterior (A, E), lateral (B, F), posterior (C, G), medial (D, H), distal (I) and proximal (J) views. A–D and J, proximal right femur. E–I, shaft and distal epiphysis of the left femur. Abbreviations: fh, femoral head; ctf, crista tibiofibularis; exg, extensor groove; ft, fourth trochanter; fxg, flexor groove; gt, greater trochanter, lc, lateral condyle; me, medial epicondyle; mc, medial condyle; pag, proximal articular groove. Scale bars equal 10 cm.

62x79mm (600 x 600 DPI)

Figure 6. *Riojavenatrix lacustris* gen. et sp. nov., right tibia (CPI 1642), left tibia and astragalus (CPI 1638), and left fibula (CPI 1639A–B) in anterior (A, E, K, P), lateral (B, F, L, Q), posterior (C, G, M, R), medial (D, H, N, S), proximal (I, J, O) and distal (T). A–D and I, proximal end of the right tibia. E–H and J, left tibia and astragalus. K–O, shaft and proximal end of the left fibula. P–T, distal end of the left fibula. Abbreviations: asf, astragalar facet; ast, astragalus; cn, cnemial crest; fc, fibular crest; icn, intercondylar notch; ift, iliofibularis tubercle; it, incisura tibialis; lc, lateral condyle; lm, lateral malleolus; mf, medial fossa; mm, medial malleolus; sab, supraastragalar buttress. Scale bars equal 10 cm for A–O and 5 cm for P–T.

62x80mm (600 x 600 DPI)

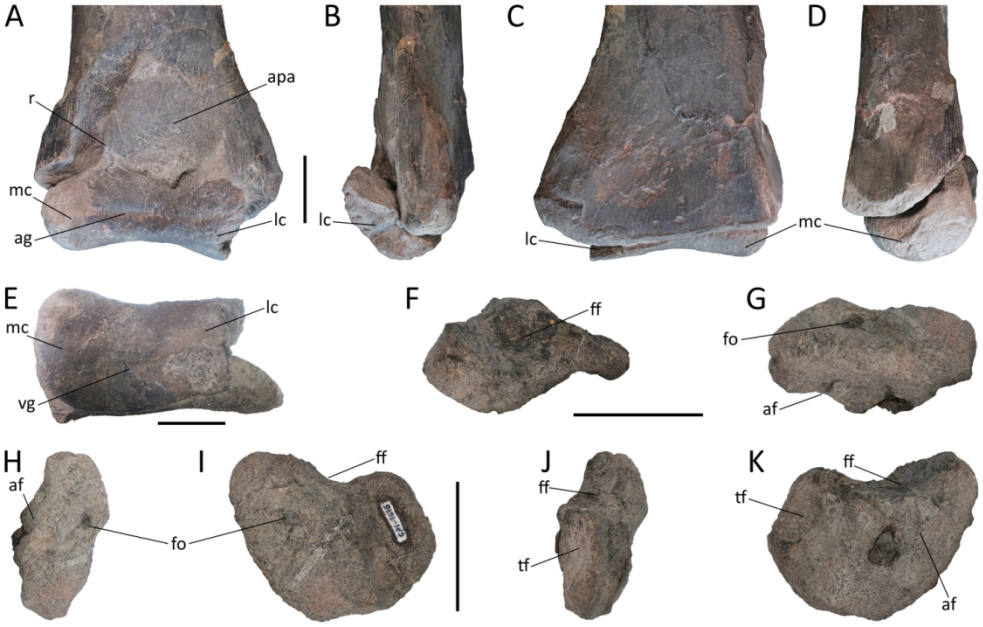

Figure 7. *Riojavenatrix lacustris* gen. et sp. nov., left astragalus and distal tibia (CPI 1638), and left calcaneum (CPI 1676) in anterior (A, H), lateral (B, I), posterior (C, J), medial (D, K), proximal (F) and distal (G). Abbreviations: af, astragalar facet; ag, anterior groove; apa, ascending process of the astragalus; ff, fibular facet; fo, foramen; lc, lateral condyle; mc, medial condyle; r, ridge; tf, tibial facet; vg, ventral groove. Scale bars equal 5 cm.

62x40mm (600 x 600 DPI)

Figure 8. *Riojavenatrix lacustris* gen. et sp. nov., left pedal elements. Metatarsal III (CPI 1640), I-2 phalanx (CPI 1647), phalanx III-1 (CPI 1645), phalanx III-3 (CPI 1646) and phalanx V-2 (or IV-3) (CPI 1648) in distal (A, L, R), dorsal (B, G, M, S, X), lateral (C, H, N, T, Y), ventral (D, I, P, V, AA), medial (E, J, Q, W, AB) and proximal (F, K, O, U, Z). A–F, left metatarsal III. G–K, left pedal phalanx I-2. L–Q, left pedal phalanx III-1. R–W, left pedal phalanx III-3. X–AB, left pedal phalanx V-2 (or IV-3). Abbreviations: ft, flexor tuberosity; ef, extensor fossa; k, keel; lc, lateral condyle; lclp, lateral collateral ligament pit; lg, longitudinal groove; lpvf; lateral proximoventral fossa; mc, medial condyle; mclp, medial collateral ligament pit; mpvf; medial proximoventral fossa; pdl, proximodorsal lip. Scale bars equal 5 cm.

62x81mm (600 x 600 DPI)

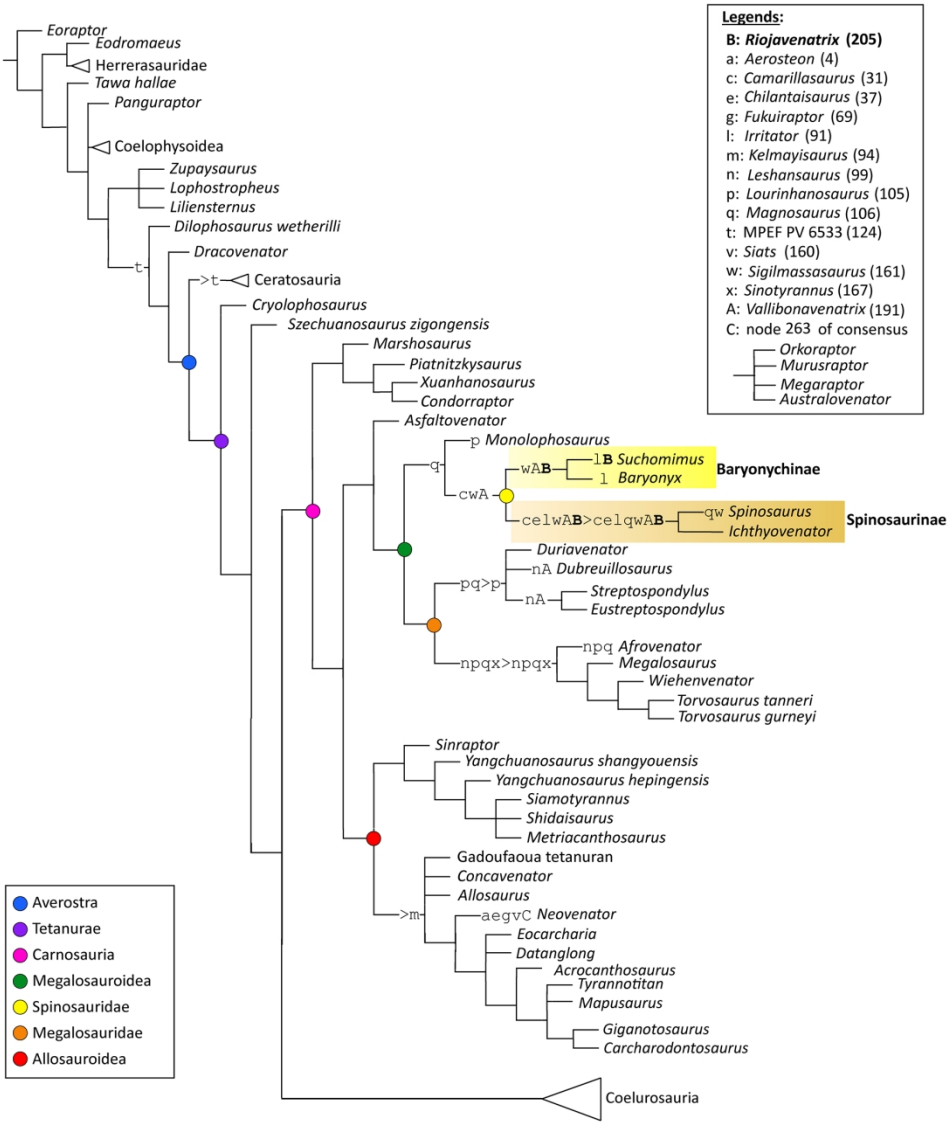

Figure 9. Phylogenetic results showing the phylogenetic position of *Riojavenatrix* based on the matrix of Rauhut & Pol (2021). Reduced consensus by iterPCR obtained from the 10000 MPTs. Alternative placements of *Riojavenatrix* and other pruned taxa are indicated by letters and indicated in the legends (right up). The coloured nodes indicate the main clades (legends in left down).

167x197mm (300 x 300 DPI)

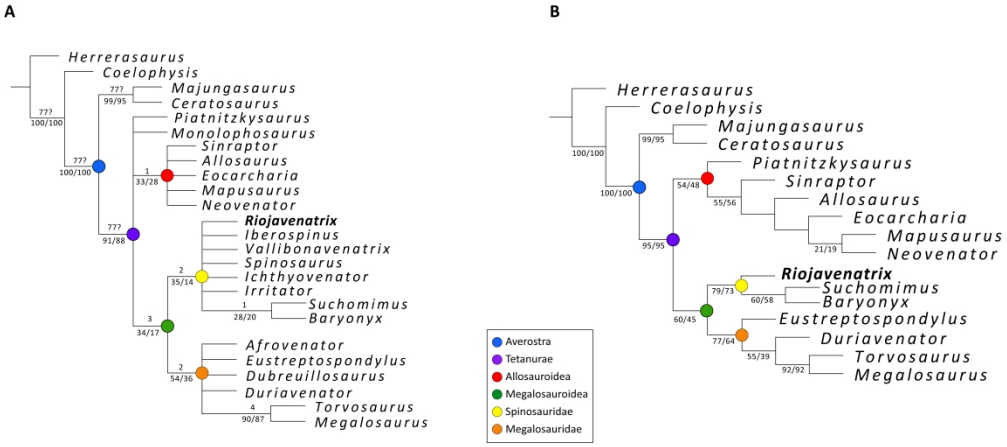

Figure 10. Phylogenetic results showing the phylogenetic position of *Riojavenatrix* based on the matrix of Mateus & Estraviz-López (2022). A. Strict consensus obtained from 307 MPTs. Bremer support values are up to the nodes, and Jackknife and bootstrap values are down to the nodes. B. Reduced consensus by agreement subtree methodology with 16 taxa, Jackknife and bootstrap values are down to the nodes. The coloured nodes indicate the main clades (legends in left down).

569x251mm (300 x 300 DPI)

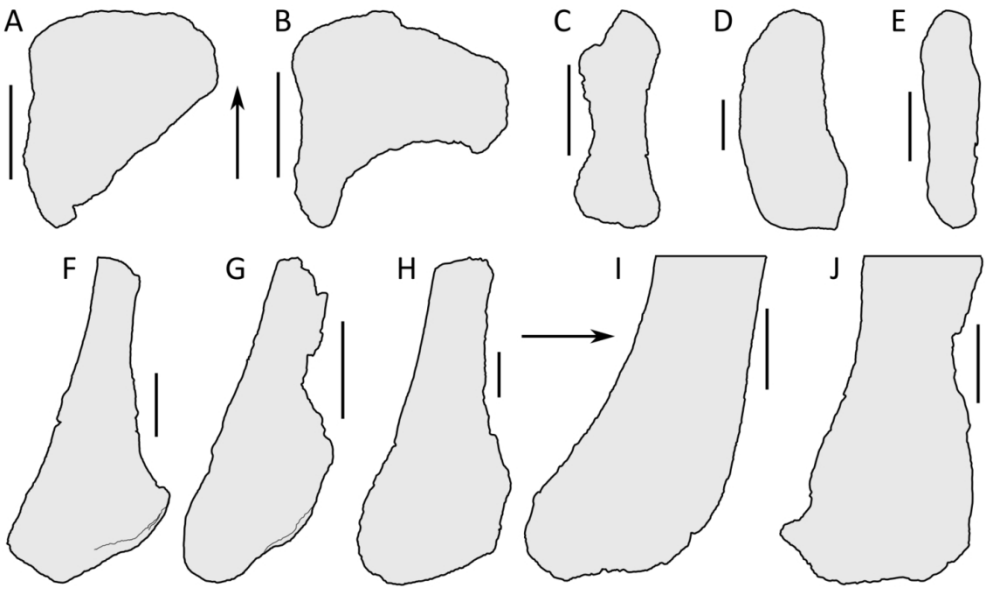

Figure 11. Comparison of spinosaurid elements with *Riojavenatrix lacustris* gen. et sp. nov. (A) left pubic boot of *Riojavenatrix* (CPI 1675A–B), (B) right pubic boot of *Ichthyovenator* (DMS BK10-11; based on Allain et al., 2012), (C) left pubic boot of *Baryonyx* (NHMUK VP R9951), (D) left pubic boot of *Suchomimus* (MNN GDF500), and (E) right pubic boot of FSAC-KK 11888 in distal view. (F) right ischial boot of *Riojavenatrix* (CPI 1641A–B), (G) right ischial boot of *Vallibonavenatrix* (MSMCa-1–3), (H) left ischial boot of *Suchomimus* (MNN GDF500), (I) left ischial boot of FSAC-KK 11888, and (J) right ischial boot of *Ichthyovenator* (DMS BK10-13; based on Allain et al., 2012) in lateral view. Note that the drawing of the pubic boot of *Ichthyovenator* (DMS BK10-11) and FSAC-KK 11888, and the ischial boot of *Suchomimus* (MNN GDF500) is a mirror image of the element. Note that the arrows point anteriorly. Scale bars equal 5 cm.

62x37mm (600 x 600 DPI)

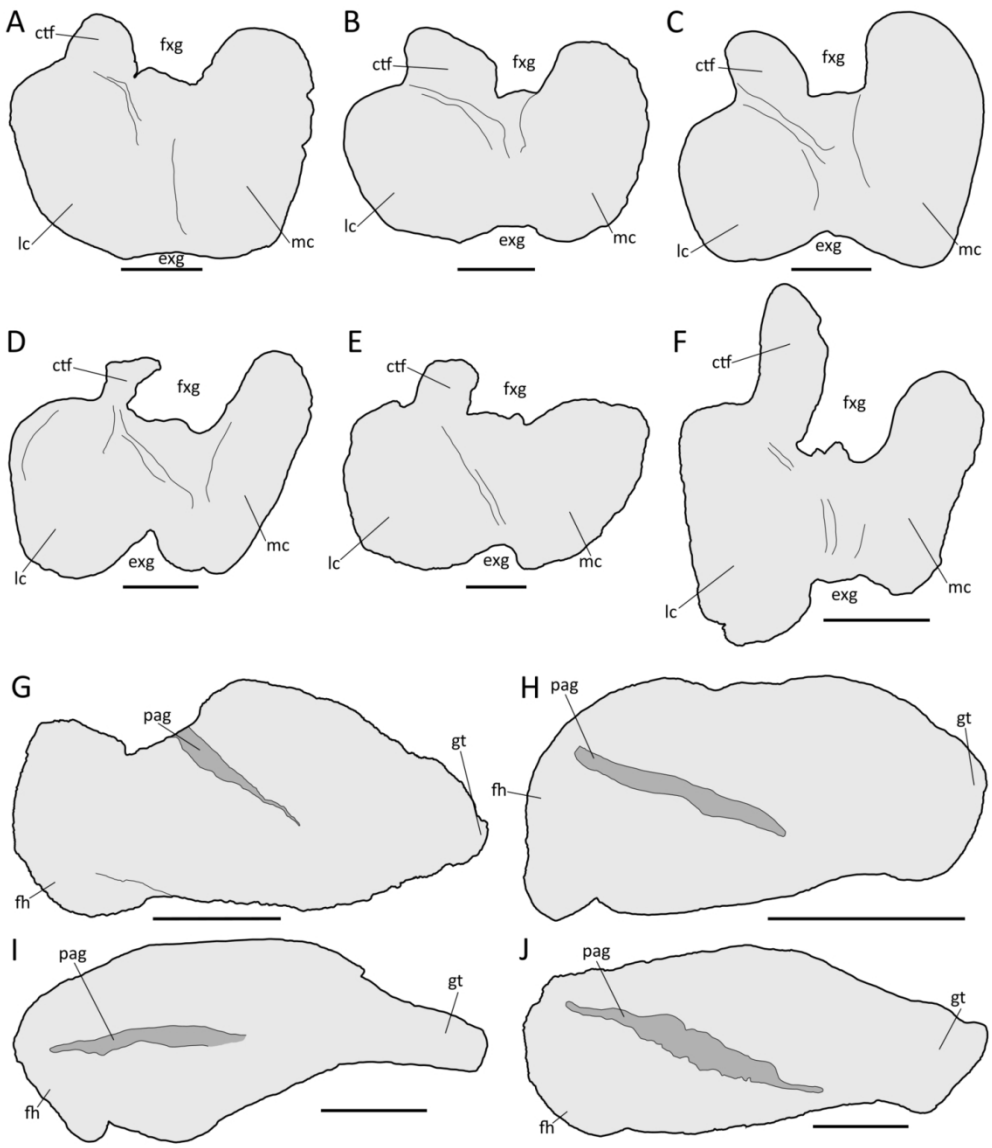

Figure 12. Comparison of spinosaurid elements with *Riojavenatrix lacustris* gen. et sp. nov. Megalosauroid femora in (A–F) distal and (G–J) proximal views. Left femur of (A) *Riojavenatrix* (CPI 1637), (E, J) *Suchomimus* (MNN GDF500) and (I) *Baryonyx* (NHMUK VP R9951), and right femur of (B) CMP-2b/21, (C) *Megalosaurus* (NHMUK PV 31806), (D) *Baryonyx* (NHMUK VP R9951), (F) FSAC-KK 11888, (G) *Riojavenatrix* (CPI 1643) and (H) CMP-MS-0/22. Abbreviations; fh, femoral head; cft, crita tibiofibularis; exg, extensor groove; fxg, flexor groove; gt, greater trochanter; lc, lateral condyle; mc, medial condyle; pag, proximal articular groove. Note that the drawings of *Baryonyx* (NHMUK VP R9951), *Suchomimus* (MNN GDF500) in proximal view, and *Baryonyx* (NHMUK VP R9951), *Megalosaurus* (NHMUK PV 31806), CMP-2b/211 and FSAC-KK 11888 are mirror images of the elements. Scale bars equal 5 cm.

62x72mm (600 x 600 DPI)

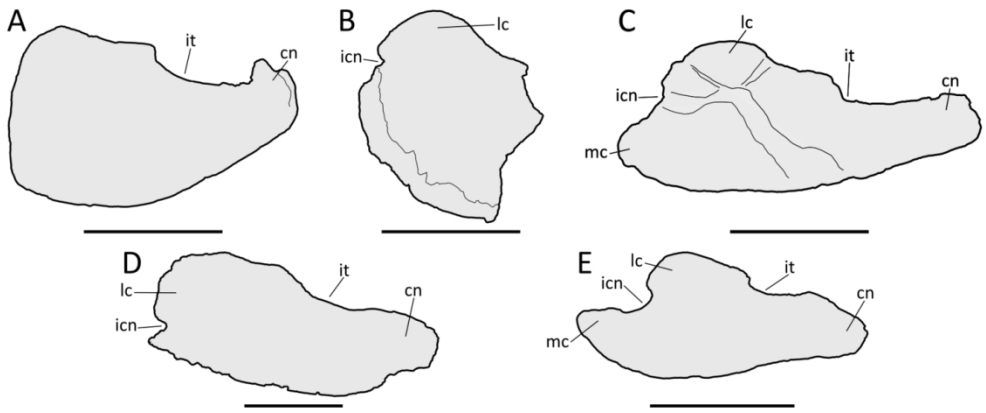

Figure 13. Comparison of spinosaurid elements with *Riojavenatrix lacustris* gen. et sp. nov. Left tibia of (A) *Riojavenatrix* (CPI 1638) and (D) *Suchomimus* (MNN GDF500), and right tibia of (B) *Riojavenatrix* (CPI 1642), (C) *Camarillasaurus* (MPG-KPC8) and (E) FSAC-KK 11888 in proximal view. Abbreviations: cn, cnemial crest; icn, intercondylar notch; it, incisura tibialis; lc, lateral condyle; mc, medial condyle. Note that the drawings of *Camarillasaurus* (MPG-KPC8), *Riojavenatrix* (CPI 1638) and FSAC-KK 11888 are mirror images of the elements. Scale bars equal 10 cm.

62x26mm (600 x 600 DPI)

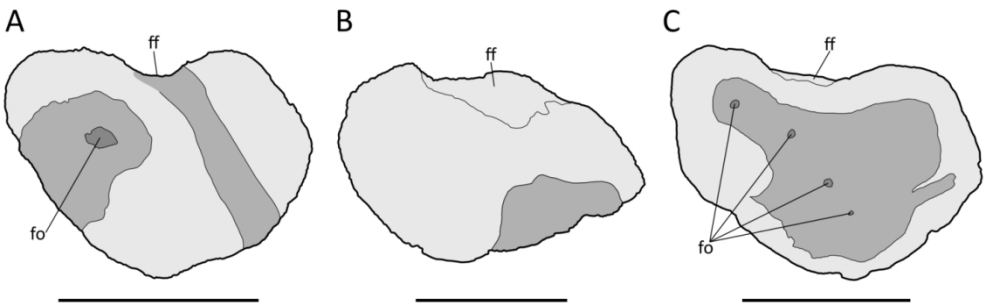

Figure 14. Comparison of spinosaurid elements with *Riojavenatrix lacustris* gen. et sp. nov. Left calcaneum of (A) *Riojavenatrix* (CPI 1676) and (B) *Iberospinus* (ML1190-31; based on Mateus & Estraviz-López, 2022), and right calcaneum of (C) *Baryonyx* (NHMUK VP R9951) in lateral view. Abbreviations: ff, fibular facet; fo, foramen. Note that the drawing of *Baryonyx* (NHMUK VP R9951) is a mirror image of the element. Scale bars equal 5 cm.

62x19mm (600 x 600 DPI)

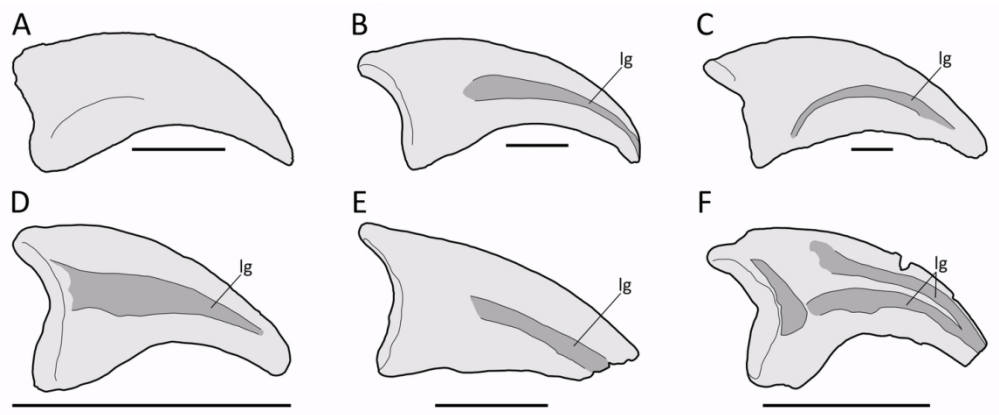

Figure 15. Comparison of spinosaurid elements with *Riojavenatrix lacustris* gen. et sp. nov. Left I-2 pedal phalanx of (A) *Riojavenatrix* (CPI 1647) and (F) *Deinonychus* (YPM 5205), and right I-2 pedal phalanx of (B) Carcharodontosauria indeterminate (SHN.019), (C) *Tyrannosaurus* (FMNH PR2081; based on Brochu, 2003), (D) *Bambiraptor* (AMNH 30556) and (E) *Alectrosaurus* (AMNH 6554) in medial view. Abbreviations: lg, longitudinal groove. Note that the drawing of *Alectrosaurus* (AMNH 6554), *Bambiraptor* (AMNH 30556), *Tyrannosaurus* (FMNH PR2081) and the indeterminate carcharodontosaurian (SHN.019) are mirror images of the elements. Scale bars equal 2 cm, but for D, which is 1 cm.

62x26mm (600 x 600 DPI)

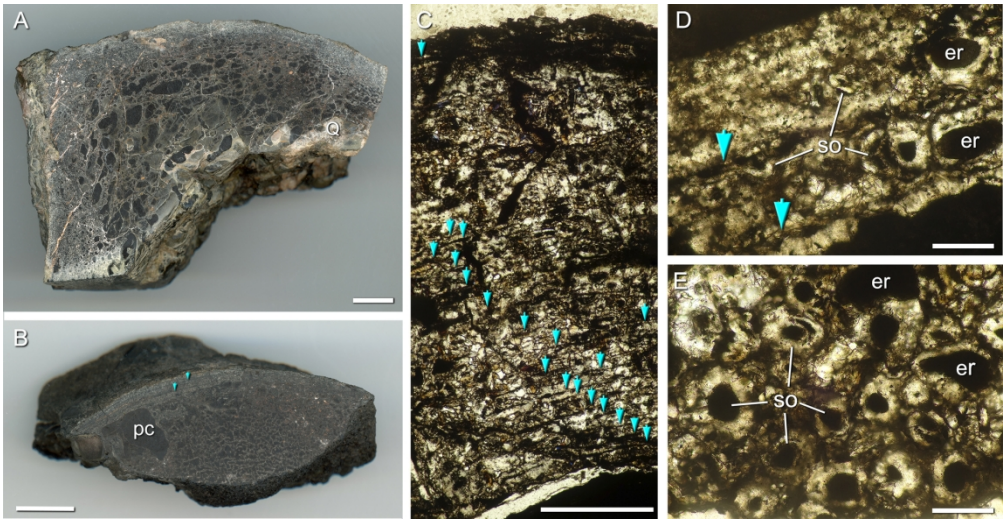

Figure 16. Histological preparations of *Riojavenatrix lacustris* gen. et sp. nov. material. A, polished cross-section of a possible fragment of the proximal right femur (CPI 1643) in ventral view, showing a thin cortex enclosing a medullary cavity invaded by bony trabeculae of cancellous bone. B, transverse polished section of a fragmentary vertebral centrum showing an internal pneumatized internal structure. Note the presence of a couple of lines of arrested growth visible even to the naked eye (blue arrowheads). C, transverse thin section of the cortical bone of the same specimen, showing a clear pattern of stratification produced by the cyclical presence of lines of arrested growth (blue arrowheads). D, transverse thin section of the externalmost cortex of a fragmentary dyaphyseal limb bone fragment, showing two well-preserved lines of arrested grow (blue arrowheads), several isolated secondary osteons and oval erosion rooms (note that these resorption cavities are surrounded only by a single coat of lamellar bone tissue, remaining as open, incipient secondary osteons). Bone surface is on the top. E, same thin section showing intense remodelation in the internalmost cortex. Only two generations of secondary osteons are observed. Although densely packed, secondary osteons overlap each other very little. Abbreviations: pc, pneumatic cavity; Q, quartz cement; er, erosion room; so, secondary osteons. Photographs B–D in plane polarized light. Scale bars equal 1 cm for A, 0.1 mm in B and C, and 1 mm in D.

168x86mm (300 x 300 DPI)